BEE-DRONES: Ultra low-power monitoring systems based on unmanned aerial vehicles and wake-up radio ground sensors

(Article begins on next page)

09 August 2024

BEE-DRONES: Ultra Low-power Monitoring Systems based on Unmanned Aerial Vehicles and Wake-up Radio Ground Sensors

Angelo Trotta[a,1], Marco Di Felice[a,c], Luca Perilli[b,c], Eleonora Franchi Scarselli[b,c], Tullio Salmon Cinotti[a,c]

[a]*Department of Computer Science and Engineering, University of Bologna, Italy*
[b]*Department of Electrical, Electronic, and Information Engineering, University of Bologna, Italy*
[c]*Advanced Research Center on Electronic Systems "Ercole De Castro" - ARCES, University of Bologna, Italy*

Abstract

Nowadays, Unmanned Aerial Vehicles (UAVs) represent a significant aid on scenarios where fixed, ground infrastructures are temporarily or permanently not available; this is the case of large-scale applications of the Internet of Things (IoTs), e.g. smart city and agriculture 3.0, where the UAVs can be employed as mobile data mules and gather the data from Wireless Ground Sensors (WGSs). UAV-aided wireless sensor networks (WSNs) introduce considerable advantages both in terms of performance and costs since they avoid the need of error-prone multi-hop communications, and also the installation of static gateways; at the same time, they pose formidable research challenges for their implementation, like the synchronization issue between the UAV and the WGS and the path planning, which should take into account the extremely limited flight autonomy of the UAVs. In this paper, we address both the issues above by proposing BEE-DRONES, a novel framework for large-scale, ultra low-power UAV-aided WSNs. In order to mitigate the synchronization problem, we investigate the utilization of passive Wake-up Radio (WR) technology on the WGSs, and of wireless power transfer from the UAVs: by harvesting the energy from the UAV hovering over it, the WGS is activated only for the short time required to transfer the data toward the mobile sink, while it experiences zero-consumption in sleep mode. We investigate the

---

[1]Corresponding author: angelo.trotta5@unibo.it

performance of passive WR-based WGS through real measurements, under different WGS-UAV distances and antenna orientations. Then, based on such results, we formulate the joint WGS scheduling and UAV path planning problem, where the goal is to determine the optimal trajectory of the UAVs activating the WR-based WGSs while taking into account the Value of the Sensing (VoS) as well as the total lifetime of the WSN. The original problem is transformed into a multi-commodity flow problem, and both centralized and distributed heuristics over the multi-graph are proposed. Finally, we evaluate the proposed algorithms through extensive OMNeT++ simulations; the results demonstrate the gain of `BEE-DRONES` in terms of extended lifetime compared to traditional, non WR-based solutions (e.g. duty-cycle), and in terms of reduced data-correlation compared to non VoS-aware path planning solutions.

1. Introduction

1.1. Goal

According to recent studies, the global market of sensors is expected to grow with a compound annual rate (CAGR) of 11.3 percent until 2022, when the market will reach
5 241 billion of dollars[2]. The rising demand is mainly driven by the Internet of Things (IoT) and by its vertical applications [1]; in some cases, like in smart-cities and agriculture 3.0, the deployment of monitoring systems on large-area is required, and the likely big amount of sensor data are then processed and analyzed via Machine Learning (ML) approaches. Hence, the energy-efficiency of the sensing devices becomes a fundamen-
10 tal requirement both in terms of cost-effectiveness and system maintainability. To this purpose, Wake-up Radio (WR) technology represents one of the most promising solution towards ultra low-power IoT nodes [2]. The main idea of WR is to introduce an additional circuitry able to switch on the main radio when detecting an incoming transmission (the wake-up signal) [2]; moreover, in passive mode, the WR device is able
15 to harvest the energy from the radio transmissions of an external transceiver, hence

---

[2]Source: https://www.i-scoop.eu/global-sensor-market-forecast-2022/

achieving true-zero consumption in sleep state [3]. At the same time, the potential of passive WR technology is constrained by the reduced operative range of the devices and the consequential need to provision an high number of WR transmitters on large-scale IoT scenarios, with a negative impact on system cost and scalability. In this paper,

20 we aim to circumvent such drawback by investigating how to deploy ultra low-power, large-scale IoT monitoring systems based on the integration of UAVs and WR-based wireless ground sensors (WGSs); each UAV serves as a WR transmitter, i.e. it transfer energy to wake-up a specific WGS, and as a data mule, i.e. it gathers the data sent from the same WGS. Specifically, we address two joint issues: (*i*) what is the performance

25 gain offered by WR technology over state-of-the-art solutions (e.g. duty-cycle) and its suitability for UAV-WGS communication links? and, consequently, (*ii*) how to design optimal joint WR-based WGS scheduling and UAV path-planning policies able to meet the requirements of the IoT monitoring systems?

1.2. Context and Motivations

30 UAV-aided Wireless Sensor Networks (WSNs) have been largely investigated in the literature [4]. Several studies demonstrated the advantages of using mobile sinks for low data-rate sensing applications, or investigated the combined usage of aerial and ground multi-hop communications [5]. At the same time, the practical deployment of UAV-aided WSNs poses additional challenges that are far from being addressed. First,

35 the trajectory of the UAVs must be carefully determined on large-scale scenarios due to the limited autonomy of the devices, which is in the order of few tens of minutes even on top commercial hardware. The UAV path-planning can be considered an instance of the Travelling Salesman Person (TSP) problem, and hence several heuristics have been proposed [6][7][8]. However, most of them focuses on the overall energy

40 consumption of the UAVs induced by the mobility or on the energy consumption of the WGSs induced by the wireless communication, while few studies take into account the effective requirements of the sensing applications which must process the sensing data [9][10][11]. Second, UAV-aided WSNs must face the synchronization problem, i.e. how the WGSs can be aware of the UAV transit and of the consequential transmis-

45 sion opportunity. UAV-initiated solutions require the WGSs to be always active, which

3

is not practical for battery-constrained devices [12][13]; vice versa, WGS-initiated solutions assume strict temporal synchronization between the UAV and the WGS, and consequently they are not easily deployable.

1.3. Contributions

In this paper, we address both the data-quality and the synchronization issues mentioned above, by presenting BEE-DRONES, a novel framework for energy-efficient data collection on generic UAV-aided WSNs. We consider a scenario where the WGSs are equipped with the passive wake-up radio circuitry described in [3] and -like the title suggests- we assume that UAVs will mimic the pollination process operated by bees, i.e. they hover over a selected WGS, and transfer energy in order to wake-up the device, thus solving the synchronization issue with no energy overheads for the WGS. Also, in BEE-DRONES, the UAVs are able to provide persistent aerial coverage of the scenario, by scheduling their recharge operations on charging stations placed on the ground. We provide four main contributions in this study:

- We review the architecture of our WR-based WGS prototype [14], and we show, by experimental results, the performance gain introduced by the passive WR technology compared to traditional duty-cycle mechanisms. Also, we provide insights of the wake-up operations for different UAV heights and antenna models and orientations.

- We move from the single UAV-WGS link to a WSN network empowered by UAVs, and we address the general problem of determining the optimal trajectory of each UAV, by modeling the energy harvesting process, the UAV and WGS battery consumption and the WGS-UAV communication. Differently from previous studies, the optimization problem takes into account the quality of the sensing data -called Value of Sensing (VoS) in the following- expressed through the correlation of different sensor readings on spatio-temporal dimension, i.e.: at each flight, the UAVs must maximize the scenario coverage of the readings, while avoiding discharging always the same WGSs. We considerably extend the preliminary optimization framework presented in [14] by modeling the UAV po-

4

sitioning and orientation errors as well as the communication protocol between the UAV and the WGS.

- Given the NP-hardness of the optimization problem, we rewrite it as a multi-commodity flow problem on a multi-graph; we determine the optimal UAV altitude and hovering time so that the probability of activating a WGS and of gathering the sensor data from it are both higher than pre-defined thresholds. Then, we propose a centralized heuristic over the multi-graph that computes the charging time and the list of WGSs to query during the path for each UAV, assuming de-synchronized operations among them. Finally, we derive a distributed path planning algorithm which relies on local information sharing among the UAVs; hence, this solution is robust also in case of UAVs malfunctioning or of time-varying scenario conditions.

- We evaluate the performance of centralized and distributed BEE-DRONES algorithms on simulated OMNeT++ scenarios. The impact of several parameters (e.g. WGSs density, UAVs availability, data correlation parameters) on the overall system lifetime, and on the VoS metric are investigated. Finally, we compare them against other path-planning strategies and traditional, non WR-based solutions for the WGSs.

The simulation analysis reveals that both centralized and distributed BEE-DRONES solutions are able to maximize the data utility compared to basic path planning strategies, and that the usage of WR technology produces a lifetime enhancement up to +30% more than duty-cycle mechanisms. The rest of the paper is structured as follows. Section 2 provides an extensive survey of related works on UAV-aided WSNs, and on the few recent studies integrating the WR technology on the loop. Section 3 provides experimental results of the WR-WGS technology on a single communication link. Sections 4 and 5 introduce respectively the system model and the optimization problem. Section 6 revises the problem formulation by using multi-commodity flow theory and it describes the BEE-DRONES algorithms. Section 7 shows the OMNeT++ simulation results of the proposed solutions. Section 8 draws the conclusions and discusses the future research activities.

5

2. Related Works

UAV-aided wireless sensor networks are a well investigated topic; however, few studies have considered the usage of WR technology for UAV-WGS communications. We review the literature by classifying the existing studies into three main categories, i.e. works focusing on WGS-UAV communication, on the UAV path planning for the sensor data acquisition and finally on UAV-aided WR-based sensor networks.

2.1. WGS-UAV communication

We further distinguish between studies characterizing the Aerial-to-Ground (AtG) link at the PHY layer [20][26][27], and studies investigating how to coordinate the ground-aerial transmissions at the MAC layer [12][13][21]. Regarding the AtG link performance analysis, we cite the measurements in [20] that demonstrate that the classical two-ray path loss model is not accurate at large UAV-WGS distances. Some interesting theoretical results can be found in [26] and [27]; in [26], the authors compute the the optimal UAV speed and WGS transmitting power so that the overall aviation time needed to gather the data from sensors placed on a line is minimized. In [27], the per-node capacity of a WSN covered by one or multiple UAVs is derived. Similarly, novel MAC strategies are requested to cope with the mobility of the UAVs, the limited duration of the transmission opportunity and the possible large number of WGSs attempting to access the channel at the same time. To this purpose, the MAC protocol proposed in [12] and [13] introduces a priority-based data acquisition mechanism mapping the contention window of the IEEE MAC 802.11 protocol to the position of WGSs inside the UAV's coverage area. Similarly, multiple priority-based data acquisition strategies for UAV-WGS communication are investigated in [21]: the simulation results demonstrate that the system performance are maximized when using a joint policy that takes into account the contact duration time and the data-rate on each AtG link. Cooperative diversity techniques are proposed and evaluated in [22] and [23]. Sensor clustering is another approach to reduce the number of AtG transmissions at each UAV transit and hence to mitigate the MAC collisions; to this purpose, [24] investigates the optimal balance of multi-hop ground forwarding and aerial communications, based on
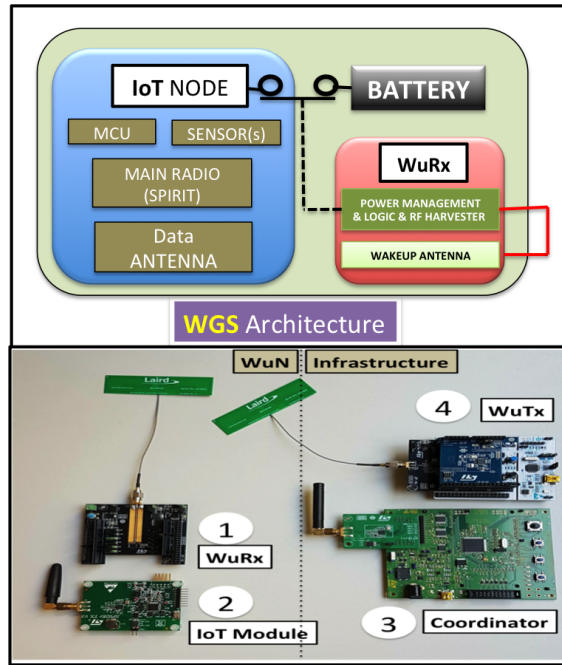
Figure 1: The architecture of the WGS with Passive WR technology (top) and its current implementation on the WuRx (bottom left) and WuTx (bottom right) devices are depicted.

a latency-energy tradeoff. Finally, the study in [25] evaluates the performance of a ContikiMAC-based UAV-WGS data acquisition strategy on a small testbed.

2.2. UAVs Path planning and data acquisition strategies

Determining the optimal path of a fleet of UAVs visiting a set of WGSs is a challenging problem due to the constrained maneuverability and limited autonomy of the UAVs, as well as to the reduced communication range of the WGSs. In [6], the authors demonstrate that the optimal UAV trajectory consists of connected line segments and hence it can be modeled as an instance of the Traveling Salesman Problem (TSP). Several heuristics have been proposed: in [7], a solution based on the Ant Colony Optimization (ACO) is discussed for farmland information monitoring, while an iterative procedure based on the Dijkstra algorithm is described in [8]. In [28], the constrained maneuverability of the UAVs is taken into account in order to transform a TSP tour into a smoother path. Clustering-based path planning strategies are proposed in [30] and

7

[29]; specifically, the goal of [30] is to define the trajectory of each UAV as a series of waypoints rather than of WGSs, so that the overall network energy consumption is minimized. A special instance of path planning problem is when the position of the WGSs is unknown; in [31], different strategies to sweep the playground are surveyed, while in [32] the UAVs employ POMDP techniques to discover the optimal strategy (i.e. their trajectories) in post-disaster applications. Since the path planning is often formulated as an optimization problem, another way to classify the existing studies is based on the goal function. In [33], the aim is to minimize the maximum energy consumption of the WGSs, while modeling the reliability of the AtG links under fading conditions. In [34], the authors propose a multi-objective path-planner, where the utility function is a combination of data-related, energy-related, time-related and risk-related metrics. In [35], the optimization problem aims to guarantee that the minimal capacity of the aerial link is always greater than a QoS threshold, and that the aerial network is always connected to a ground station. In [9] and [10], the path planning problem takes into account the quality of the data gathered from the WGSs: specifically, the utility function in [9] expresses the freshness of the data, defined as the time elapsed since each WGS was queried last. In [10], the application of UAVs for wildlife area monitoring is investigated; a value of information (VoI) metric including the reliability of the sensed data is used as reward of the UAVs. In [11], the authors address distributed UAV path planning strategies, by considering the eventuality of software/hardware crashes and hence the need to dynamically re-allocate the WGSs to visit among the available UAVs.

2.3. WR-based WGSs and UAVs

The WR technology constitutes the frontier of ultra low-power devices able to minimize the energy consumption in idle mode; despite the recent introduction, several architectures and implementations have been proposed so far, extensively surveyed in [2]. An example of IoT WR node is presented in [15]. In this paper, we rely on the proposal in [16]. Although some works have proposed the usage of mobile nodes as wireless charger of the WGSs (e.g. [17]), very few studies have investigated the deployment of UAV-aided sensor networks with WR capabilities. In [18], the authors characterize the energy transfer region of two WGs through a theoretical study. Em-

(a)

(b)
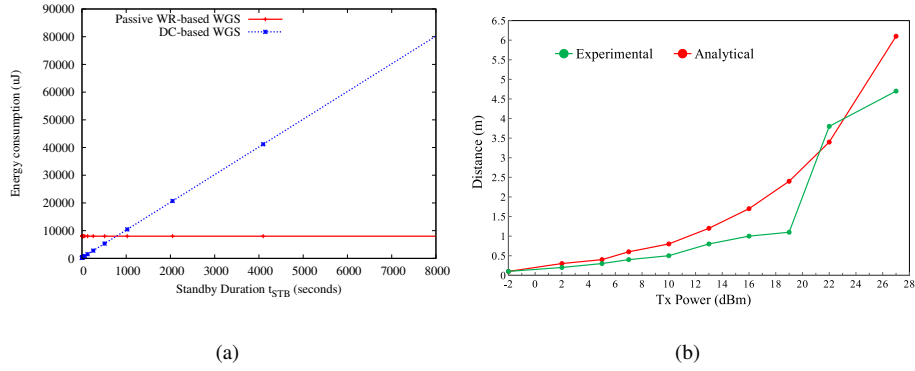
Figure 2: The energy efficiency of the passive WR-based and Duty-Cycle (DC)-based WGS, when varying the standy interval (t_{STB}) between consecutive sensor readings is shown in Figure 2(a). The operative range of the passive WR-based WGS for different transmission power values is reported in Figure 2(b).

(a)

(b)
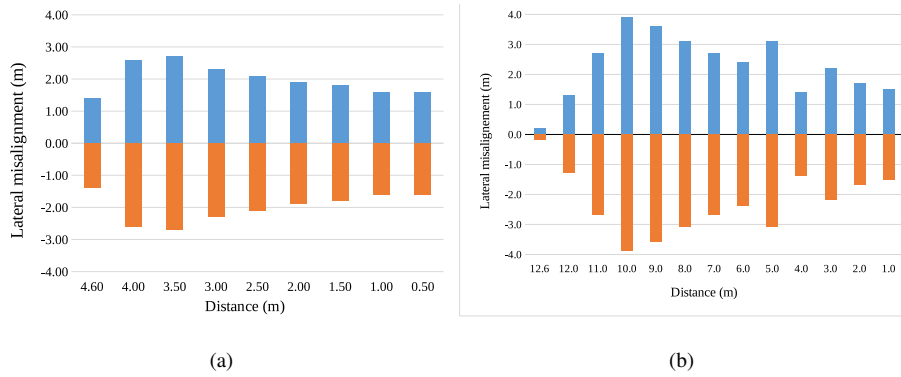
Figure 3: The maximum lateral displacement between the WuTx and WuRx device is shown in Figure 3(a). The maximum lateral displacement between the WuTx and the WuRx device equipped with a Yagi antenna with 7.3 dBi is shown in Figure 3(b).

pirical measurements are conducted in [19]; here, the authors measures the output DC voltage harvested by the WGS for different UAV heights and speeds.

3. Measurements and Motivations

180   The WGSs used in this study implement the WR architecture described in [3][16]. They are composed of three main hardware blocks, as depicted in Figure 1: a battery, a Wake-up Receiver (WuRx) module, and an IoT node. This latter includes sensors,

9

Table 1: Average energy consumption values

	Passive wake-up	**Duty-cycle**
E_{ON}	494 μJ	225 μJ
E_{STB}	0	10 $\mu W \cdot t_{STB}$
E_{BOOT}	7.5 mJ	0

a radio device for data communication and a dedicated antenna. The WuRx circuit is in charge of detecting signals from the Wake-up Transmitter (WuTx), and of re-activating the IoT module accordingly. The overall architecture supports two main operative modes, i.e. an Active class, where the the WuRx is powered by the internal battery, and a Passive Class, where the WuRx is able to harvest energy from an external RF source generated by the WuTx. Differently from our previous studies [3][14], we focus here on Passive WR-based WGS, since it represents the most energy efficiency solution. From Figure 1 we can notice that the power supply of the IoT node can be dynamically enabled/disabled by acting on a hardware switch. As a result, when the switch is off, the consumption in standby state (E_{STB}) is zero, i.e. the WGS is totally powered down; vice versa, an overhead is induced at each boot, both in terms of energy (E_{BOOT}) and time (t_{BOOT}). We used a prototype implementation of the WuRx radio [16] provided by STMicroelectronics. The WuRx is composed of a radio with a sensitivity of -18 dBm at 868MHz in Passive Mode or -38 dBm at 868MHz in Active Mode, an RF to DC energy transducer (RF energy harvester), an adjustable Low Dropout (LDO), and an ultra-low power management unit. The IoT module includes an ultra-low power microcontroller (STM32L1[3]), a subGHz radio device for data communication (SPIRIT1[4]), a battery and a temperature sensor (STTS751[5]). The microcontroller acquires the temperature data and implements the communication data link based on DASH7 standard in request/response mode. Table 1 shows the average measured values of the energy parameters for different operations, i.e. E_{ON} (trans-

---

[3]Datasheet: http://www.st.com/resource/en/datasheet/stm32l151c6.pdf

[4]Datasheet: http://www.st.com/resource/en/datasheet/spirit1.pdf

[5]Datasheet: http://www.st.com/resource/en/datasheet/stts751.pdf

mit state), E_{STB} (standby state), E_{BOOT} (boot state). On the same Table, we include

the results when the IoT module (STM32L1+SPIRIT1) implements a duty-cycle (DC)

mechanism without employing any WR technology. Based on these values, Figure

2(a) compares the passive WR and DC solutions in terms of average energy consump-

tion for an ON-OFF transition (wake-up, transmission and standby phase): on the x

axis, we varied the sleep length (t_{STB}). For very short t_{STB} values, the DC class

has the lowest average consumption since it avoids the boot operations; vice versa,

the energy consumption increases significantly for $t_{STB} > 1000$ seconds. However,

it is worth remarking that: (*i*) in typical UAV-based WSN applications, the interval

between consecutive sensor readings can be quite long; (*ii*) we assumed perfect tempo-

ral synchronization between the DC length and the UAV transit, which is unpractical

to achieve, and hence additional energy overhead should be considered for the DC

case. For $t_{STB} > 1000$ seconds, the passive WR is the most energy-efficient solution

and more important it intrinsically solves the UAV-WGS synchronization problem. On

Figure 2(b), we depict the maximal distance at which it is possible to wake-up the

WGS with 100% probability of success; on the x-axis, we vary the transmitting power

of the WuTx. We did not introduce the mobility factor, hence both WuTx and WuRx

are at fixed positions. On the same Figure we also show the maximum distance com-

puted through the well-known Friis model, introduced later in Section 4.3 (Equation

2). We found experimentally that each WuRx device needs a minimum received en-

ergy of $E^{\mathrm{WU}} = 633.6nJ$ to be powered on. We can notice from Figure 2(b) that the

analytical results follow quite strictly the experimental results. Moreover, the max-

imum achievable distance on the UAV-WGS link does not exceed 5 meters, for the

configuration with the maximum power (P_{wu}=27dBm). Hence the operative range for

passive WR-based WGSs is considerably lower than the active case [14]; however, the

energy overhead introduced by the WR circuitry is equal to zero in idle mode. Also,

the range between the UAV and WGS can be extended through the utilization of di-

rectional antennas, as further investigated below. In the experimental measurements

reported in Figures 2(b), 3(a) and 3(b), we arranged the WuRx (assuming it is on the

ground) and the WuTx (assuming it is on the UAV) on two supports at a height of 1.7

m from the ground in the line-of-sight condition, to be sure that the ground is out of

11

the Fresnel zone, avoiding interferences and power loss. This experimental setup emulates with a good approximation the real conditions in which the UAV hovers over the WGS; the distances on the straight-path we measured in the plane parallel to the ground correspond to the vertical distances (perpendicular to the ground), i.e. altitude, in the real conditions with UAVs and WGSs. In the previous analysis, we assumed the WGS and UAV to be perfectly aligned vertically during the hovering phase; however, this assumption might not be completely realistic if we take into account positioning (e.g. induced by the GPS) or controller errors on the UAV. To this aim, Figure 3(a) investigates the performance of the wake-up operations when varying the displacement between the WuRx and WuTx antennas; more in detail, we varied on the x axis the distance on the straight-path between WuRx and WuTx devices (corresponding to the altitude between UAV and WGS), while on the y axis we reported the maximum lateral misalignment, with respect to the straight-path between WuRx and WuTx, on the left (blue bars) and right (orange bars, clearly symmetric to the blue ones) at which the wake-up process is successfully completed with 100% of probability. To better explain the figure, the zero in the y axis represents the straight-path between WuRx and WuTx, and the blue and orange bars represent the area in which the wake-up process can successfully happen. We used omni-directional antennas with gain $G_{\max}^{\mathrm{rx}} = G_{\max}^{\mathrm{tx}}$=1dBi. The maximum lateral misalignment (2.5m) is achieved for a distance of 3.5 meters, that translated into angles corresponds to a maximum irradiation cone $\alpha_{\max}^{\mathrm{tx}}$ equal to 1.314rad. In Figure 3(b), we repeated the range analysis when considering a different antenna on the WuTx device with maximum gain equal to 7.3dBi and irradiation cone $\alpha_{\max}^{\mathrm{tx}}$ equal to 0.743rad. The peaks at 3m and 5m show the antenna side lobes. Comparing the results of Figures 3(a) and 3(b), we can notice that the operative range of passive WR technology increases to up to 12 meters: hence, the flying altitude of the UAVs can be properly tuned according to the antenna model of the WGSs. However, this introduces a trade-off with the UAV positioning accuracy and WGS wake-up probability, which is modeled in the Section below.

4. System Model

Without loss of generality, we consider a generic scenario of size $M \times M$ including
WGSs, UAVs and charging stations (see Figure 4). The system evolves over ordered
time slots $T = \{t_0, t_1, \ldots, T_{\text{LIMIT}}\}$ where each $t_k \in T$ has length of t_{slot} seconds.
Let $S = \{s_1, s_2, \ldots, s_{N_S}\}$ denote the set of WGSs, deployed at fixed scenario loca-
tions; each $s_j \in S$ is composed of a passive wake-up receiver (WuRx) and a main
radio interface to send the sensed data to the UAV. We assume that each WuRx device
needs an amount of E^{WU} energy to be powered on, in accordance with the experi-
mental results depicted in Figure 2(b). In addition, we deploy a fleet of N_U UAVs
$U = \{u_1, u_2, \ldots, u_{N_U}\}$. Each UAV is equipped with a wake-up transmitter (WuTx),
a radio interface to receive data from the WGSs and a localization system for self-
positioning. We do not make any assumption on the wireless technology (WiFi, BLE,
etc) used on the GtA link. Similarly, we assume that the UAV will be in charge of
storing the data, and of uploading them on a remote server by means of a 4G connec-
tion. In absence of cellular coverage, multi-hop communication among UAVs might be
employed [36][37], also envisaging the usage of DTN-based solutions (e.g. [38]) given
the sporadic nature of wireless contacts among the UAVs on large-scale environments.
However, routing and UAV network topology management are not considered in this
study since its focus is on the low-power WGS-UAV data gathering.

In order to guarantee a persistent aerial coverage of the environment, we assume the
presence of N_U charging stations $C = \{c_1, c_2, \ldots, c_{N_U}\}$ uniformly distributed in the
scenario, and providing wireless recharge to each UAV lying on its surface. Let $P_{\text{rec}}^{\text{C}}$
be the charging power of each $c_i \in C$, assumed equal for all the stations; we consider
the basic case where there is one dedicated charging station for each UAV. Charging
scheduling algorithms like the one described in [40] can be used otherwise. While
not charging, each UAV u_i at time slot t_k moves at an altitude of $h_{u_i}^{t_k}$ meters from the
ground. Finally, let p be the function defining the position of each WGS, of the UAVs
and the charging stations at each time slot $t_k \in T$. At system start-up, $p(u_i, t_0) = p(c_i)$
(i.e. the UAVs are located at the charging stations); the positions of these latter ($p(c_i)$)
and of the WGSs ($p(s_j)$) are assumed fixed and uniformly distributed over the sce-
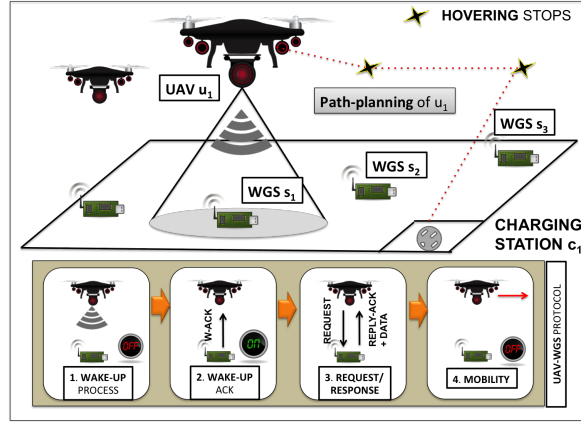
Figure 4: The UAV-aided WSN scenario considered in this study.

nario. In Table 2 the main system variables used in this paper are listed with a short description. In the following, we further detail the system model in terms of UAV mobility (Section 4.1), antenna characteristics (Section 4.2), energy transfer (Section 4.3), UAV-WGS communication and data acquisition (Section 4.4) and of the UAV and WGS energy update rules (Section 4.5).

Table 2: Symbol Table

Symbol	Meaning
M	Side of the scenario
$E(u_i, t_k), E(s_j, t_k)$	Residual energy at time t_k for UAV u_i and WGS s_j
E^{WU}	Energy required by each WuRx to wake-up
N_S	Number of WGSs
$h_{u_i}^{t_k}$	Flying altitude of UAV u_i at time t_k
$\vec{e}_{\mathrm{HOVER}}(u_i, s_j, t_k)$	Hovering error of UAV u_i over WGS s_j at time t_k
$\vec{e}_{\mathrm{LOC}}(u_i, t_k)$	Localization error of UAV u_i at time t_k
f	Wake-up signal frequency
$\alpha_{\max}^{U}$	Maximum irradiation angle for UAVs
$\alpha_{\max}^{S}$	Maximum irradiation angle for WGSs
	Continued on next page

14

Table 2 – continued from previous page

Symbol	Meaning
$G(\alpha, G_{\max}, \alpha_{\max})$	Antenna gain at angle α
Γ	Energy harvested in one time slot
t_{startup}	WGS-UAV connection setup delay
n_r	Maximum number of REQUEST retransmissions
$E_{\max}^U$	UAVs maximum battery capacity
P_{rec}^C	Charging stations' power
P_{startup}^U	Communication power during UAV startup
P_{tx}^U	Communication power during UAV transmission
$\mathcal{L}_C$	Correlation loss function
Ψ	VoS function to maximize
σ_{R}^2	Variance for the rotation error distribution
data_h	Data communication success probability
t_{slot}	Time slot length
T_{LIMIT}	Max system time
P_{wu}	WuTx transmit power
N_U	Number of UAVs
$\text{tr}_{i \leftarrow j}^{t_k}$	UAV u_i received the data from WGS s_j at time t_k
$\varrho_x^{u_i}(t_k)$	x-Rotation of the WuTx antenna at time t_k
$\varrho_y^{u_i}(t_k)$	y-Rotation of the WuTx antenna at time t_k
$G_{\max}^U$	Maximum antenna gain for UAVs
$G_{\max}^S$	Maximum antenna gain for WGSs
$P_{\text{Rx}}^{u_i, s_j}(t_k)$	Power received at WGS s_j from UAV u_i at time t_k
$\kappa(P_{\text{Rx}})$	WuRx transducer efficiency at P_{Rx} input power
t_{timeout}	Timout for REQUEST message retransmission
$E_{\text{self}}^{\eta}(e, t)$	Battery self-discharge rate at each time-slot
η	battery monthly self-discharge in percentage
$E_{\max}^S$	WGSs maximum battery capacity
	Continued on next page

Table 2 – continued from previous page

Symbol	Meaning
P_{fly}^{U}	Propulsion power of the UAV
P_{startup}^{S}	Communication power during WGS startup
P_{tx}^{S}	Communication power during WGS transmission
v_{max}	maximum UAV velocity
m_t and k_t	Coefficients modelling the temporal correlation
m_s and k_s	Coefficients modelling the spatial correlation
$\mathcal{L}_{\mathrm{BEE}}$	Loss function used in the BEE-DRONES method
$\mathbb{P}_{\mathrm{pl}}(d)$	Packet loss probability
$\sigma_{\mathrm{POS}}^{2}$	Variance for the position error distribution
$\mathrm{wu}_{h,t}$	Wake-up success probability

4.1. Hovering model

Each UAV $u_i \in U$ moves over the scenario by periodically visiting a sequence of WGSs in order to gather the sensor data from them. Let $h_{u_i}^{t_k}$ be the flying altitude of UAV u_i at each time slot t_k. Differently from previous studies assuming continuous UAV mobility (e.g. [12] and [13]), we investigate the case where the UAV hovers over each selected WGS in order to transfer energy and hence to activate it. Let $\mathrm{hov}(u_i, s_j, t_k)$ be the 2-D ground target of UAV u_i at time slot t_k while hovering above WGS s_j (we suppose that $\mathrm{hov}(u_i, s_j, t_k) = p(s_j)$). We assume that each UAV is able to geo-localize itself (e.g. via the GPS); at the same time, we model the impact of positioning errors caused by the lack of precision of the localization source and/or by the drift in hovering mode (caused by controller errors and/or by environmental conditions like the presence of wind). The localization estimation error is defined as: $\vec{e}_{\mathrm{LOC}}(u_i, t_k) = \hat{p}(u_i, t_k) - p(u_i, t_k)$, where $p(u_i, t_k)$ is the actual real position of UAV u_i at time slot t_k and $\hat{p}(u_i, t_k)$ its local estimation (e.g. the position returned by the GPS). Similarly, we define the hovering control error as: $\vec{e}_{\mathrm{HOVER}}(u_i, s_j, t_k) = \mathrm{hov}(u_i, s_j, t_k) - \hat{p}(u_i, t_k)$. The overall position error
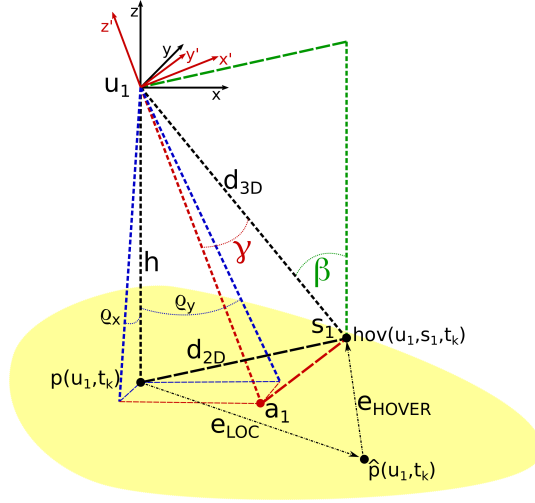
16

Figure 5: Irradiation and positioning model of UAV u_1 flying at an altitude of h meters. The rotation of $\varrho(u_1, t_k) = \langle \varrho_x^{u_1}(t_k), \varrho_y^{u_1}(t_k) \rangle$ determines a change of the coordinate reference system from $\langle x, y, z \rangle$ to $\langle x', y', z' \rangle$. The angles of irradiation for the power transmission and the reception are denoted as α and β, respectively. The irradiation area given by h, $p(u_1, t_k)$, $\varrho(u_1, t_k)$, and α_{max}^U is depicted in yellow. In Figure, $\text{hov}(u_1, s_1, t_k) = p(s_1)$.

for the UAV u_i at time slot t_k is the sum of the localization error and of the hovering error, i.e. $\vec{e}_{\text{POS}}(u_i, s_j, t_k) = \vec{e}_{\text{LOC}}(u_i, t_k) + \vec{e}_{\text{HOVER}}(u_i, s_j, t_k)$. It is easy to see that $\|\vec{e}_{\text{POS}}(u_i, s_j, t_k)\| = d_{2\text{D}}(u_i, s_j, t_k)$, i.e. the error is equal to the 2-D distance between the projected position of UAV u_i and WGS s_j. In addition, given again to external (e.g. presence of wind) or to internal factors (e.g. controller errors), we model the displacement between the UAV antenna and the WGS antenna. Let $\varrho(u_i, t_k) = \langle \varrho_x^{u_i}(t_k), \varrho_y^{u_i}(t_k) \rangle$ be the actual rotation vector of UAV u_i at time slot t_k, where $\varrho_x^{u_i}(t_k)$ and $\varrho_y^{u_i}(t_k)$ define respectively the rotation on the x and y axis. The rotation on the z axis is not considered because of the symmetric antenna model. Figure 5 shows the hovering model with the notation introduced so far.

4.2. Antenna model

Each UAV is equipped with a WuTx device and a directional antenna having maximum irradiation cone of angle α_{max}^U and maximum gain G_{max}^U. Similarly, each WGS is equipped with a WuRx and a directional antenna with maximum irradiation cone of

17

angle $\alpha_{\max}^S$ and maximum gain $G_{\max}^S$. Differently from our previous study [14], and in accordance with the experimental results of Section 3, we consider directional antennas; the antenna gain $G(\alpha, G_{max}, \alpha_{\max})[dBi]$ with a receiving/transmitting signal of angle α is modeled as in [41]:

$$G(\alpha, G_{max}, \alpha_{\max}) = \begin{cases} G_{max} + \left(-12 \cdot \left(\frac{\alpha}{\alpha_{\max}/2} \right)^2 \right) \\ \quad \text{if } \alpha \leq \frac{\alpha_{\max}}{2} \\ -\infty \quad \text{otherwise} \end{cases} \tag{1}$$

4.3. Energy transfer model

The wake-up procedure is allowed only when the UAV is hovering over the selected WGS s_j, i.e. $\mathrm{hov}(u_i, s_j, t_k) = p(s_j)$. The energy power $P_{\mathrm{Rx}}^{u_i, s_j}(t_k)[dBm]$ received by the WuRx device s_j at time slot t_k by u_i is modeled as follows:

$$P_{\mathrm{Rx}}^{u_i, s_j}(t_k) = \begin{cases} P_{\mathrm{wu}} + G(\gamma_{u_i, s_j}(t_k), G_{\max}^U, \alpha_{\max}^U) + \\ + G(\beta_{u_i, s_j}(t_k), G_{\max}^S, \alpha_{\max}^S) - \mathrm{PL}(d_{3\mathrm{D}}(u_i, s_j, t_k), f) \\ \quad \text{if } \gamma_{u_i, s_j}(t_k) \leq \alpha_{\max}^U/2 \ \wedge \ \beta_{u_i, s_j}(t_k) \leq \alpha_{\max}^S/2 \\ 0 \quad \text{otherwise} \end{cases} \tag{2}$$

where $d_{3\mathrm{D}}(u_i, s_j, t_k)$ is the actual real 3D Euclidean distance between UAV u_i and WGS s_j at time slot t_k and $\mathrm{PL}(d, f)$ is the free-space path-loss at distance d on frequency f [43]. The values of angles $\beta_{u_i, s_j}(t_k)$ e $\gamma_{u_i, s_j}(t_k)$ can be derived from trigonometry calculations as follows:

$$\beta_{u_i, s_j}(t_k) = \arccos \left(\frac{d_{3\mathrm{D}}(u_i, s_j, t_k)^2 + h_{u_i}^{t_k\,2} - d_{2\mathrm{D}}(u_i, s_j, t_k)^2}{2 \cdot d_{3\mathrm{D}}(u_i, s_j, t_k) \cdot h_{u_i}^{t_k}} \right) \tag{3}$$

$$\gamma_{u_i, s_j}(t_k) = \arccos \left(\frac{d_{3\mathrm{D}}(u_i, s_j, t_k)^2 + d(u_i, a_i, t_k)^2 - d(a_i, s_j, t_k)^2}{2 \cdot d_{3\mathrm{D}}(u_i, s_j, t_k) \cdot d(u_i, a_i, t_k)} \right) \tag{4}$$

where $d(u_i, a_i, t_k)$ is the distance between UAV u_i and the ground point a_i characterized by the maximum antenna gain having coordinates $\langle h_{u_i}^{t_k} \cdot \tan(\varrho_y^{u_i}(t_k)), h_{u_i}^{t_k} \cdot \tan(\varrho_x^{u_i}(t_k)) \rangle$ (see Figure 5), and $d(a_i, s_j, t_k)$ is the distance between the WGS s_j and the point a_i. The received power $P_{\mathrm{Rx}}^{u_i, s_j}(t_k)$ is then converted by a RF-to-DC energy transducer into an actual current that is used to activate the WGS. Let $\kappa(P_{\mathrm{Rx}})$

be the transducer efficiency of the WuRx device when receiving an input power of P_{Rx}. We consider the $\kappa(P_{\mathrm{Rx}})$ function values as defined in [39]. At each time slot t_k, the energy accumulated by WGS s_j can be computed as follows:

$$E_{\mathrm{acc}}^{s_j}(t_k) = E_{\mathrm{acc}}^{s_j}(t_{k-1}) + \sum_{u_i \in U} \Gamma(\overrightarrow{e}_{\mathrm{POS}}(u_i, s_j, t_{k-1}), \varrho(u_i, t_{k-1}), h_{u_i}^{t_{k-1}}) \quad (5)$$

where $\Gamma : \mathbb{R}^2 \times \mathbb{R}^2 \times \mathbb{R} \to \mathbb{R}$ is the transferred energy from UAV u_i to WSG s_j in one time slot:

$$\Gamma(\overrightarrow{e}_{\mathrm{POS}}(u_i, s_j, t_k), \varrho(u_i, t_k), h_{u_i}^{t_k}) = P_{\mathrm{Rx}}^{u_i, s_j}(t_k) \cdot \kappa(P_{\mathrm{Rx}}) \cdot \mathrm{t_{slot}} \quad (6)$$

and $E_{\mathrm{acc}}^{s_j}(t_k) = 0$ if no UAV is transferring energy to WGS s_j at time slot t_k. Finally, we introduce the helper function E_{check} indicating whether WGS s_j can be activated at time slot t_k, i.e. whether the received energy $E_{\mathrm{acc}}^{s_j}(t_k)$ is greater than the wake-up threshold E^{WU}:

$$E_{\mathrm{check}}^{s_j}(t_k) \quad = \quad \begin{cases} 1 & \text{if } E_{\mathrm{acc}}^{s_j}(t_k) \geq E^{\mathrm{WU}} \\ 0 & \text{otherwise} \end{cases} \quad (7)$$

4.4. Communication model

In case of wake-up process ends succesfully ($E_{\mathrm{check}}^{s_j}(t_k)$=1), the WGS s_j reads and transfers the sensor data to UAV u_i. We do not focus on the wireless technology on the AtG link, since out of the scope of the paper; instead, we model a generic request-response communication protocol with initial connection setup and message re-transmissions as depicted in Figure 4. First, the WGS acknowledges that the wake-up procedure has successfully completed by sending a `W-ACK` message to the UAV; let t_{startup} the connection setup time, assumed equal for all the WGSs. Next, the UAV sends a `REQUEST` message to the WGS and waits to receive the `REPLY-ACK` message with the sensor data piggybacked; in case no reply is received from the WGS within t_{timeout} time slots, the UAV transmits a new `REQUEST`, till a maximum of n_r attempts. We assume uniform packet dimension and that both `REQUEST` and `REPLY-ACK` messages can be transmitted and processed in one time slot (i.e. $t_{\mathrm{req}} = t_{\mathrm{rep}} = t_{\mathrm{slot}}$). Also,

we introduce the following state variables related to the communication model:

$$
\text{tr}^{t_k}_{i \to j} \;=\; \begin{cases} 1 & \text{if WGS } s_j \text{ receives the } \texttt{REQUEST} \\ & \text{from UAV } u_i \text{ successfully at time slot } t_k \\ 0 & \text{otherwise} \end{cases}
$$

355

$$
\text{tr}^{t_k}_{i \leftarrow j} \;=\; \begin{cases} 1 & \text{if UAV } u_i \text{ receives the } \texttt{REP-ACK} \text{ from} \\ & \text{WGS } s_j \text{ successfully at time slot } t_k \\ 0 & \text{otherwise} \end{cases}
$$

4.5. Battery model

Let $E(s_j \in S, t_k \in T)$ and $E(u_i \in U, t_k \in T)$ define the residual energy of each WGS and UAV at time slot t_k. We assume all the WGSs and all the UAVs to be fully charged at the system start-up, i.e. $E(s_j, t_0) = E^S_{\max}$ and $E(u_i, t_0) = E^U_{\max}$. Also, we

360 introduce the following state variables:

- *UAV state*

$$
\text{f}^{t_k}_{u_i} \;=\; \begin{cases} 1 & \text{if UAV } u_i \text{ is flying at time } t_k \\ 0 & \text{if UAV } u_i \text{ is charging at time } t_k \end{cases}
$$

- *Wake-up state*

$$
\text{w}^{t_k}_{i,j} \;=\; \begin{cases} 1 & \text{if UAV } u_i \text{ irradiates } s_j \text{ at time } t_k \\ 0 & \text{otherwise} \end{cases}
$$

- *WGS state*

$$
\text{on}^{t_k}_{s_j} \;=\; \begin{cases} 1 & \text{if WGS } s_j \text{ is ON at time slot } t_k \\ 0 & \text{otherwise} \end{cases}
$$

Similarly, we define $\text{off}^{t_k}_{s_j} = 1 - \text{on}^{t_k}_{s_j}$.

365 - *Boot and connection setup*

$$
\text{su}^{t_k}_{[u_i, s_j]} \;=\; \begin{cases} 1 & \text{if UAV } u_i \text{ or the WGS } s_j \text{ is setting the connection at} \\ & \text{time } t_k \\ 0 & \text{otherwise} \end{cases}
$$

20

- *Data communication process*

$$r_{[u_i,s_j]}^{t_k} = \begin{cases} 1 & \text{if the UAV } u_i \text{ or the WGS } s_j \text{ is in communication mode} \\ & \text{at time } t_k \\ 0 & \text{otherwise} \end{cases}$$

- *Message exchange process*

$$\text{com}_{[\text{rx,tx}],[u_i,s_j]}^{t_k} = \begin{cases} 1 & \text{if UAV } u_i \text{ or the WGS } s_j \text{ is receiving or} \\ & \text{transmitting the data packet at } t_k \\ 0 & \text{otherwise} \end{cases}$$

Based on the states above, we introduce the energy update rule for the UAVs as follows:

$$\begin{aligned} E(u_i, t_k) = \; & E(u_i, t_{k-1}) & (8) \\ & + \; (1 - f_{u_i}^{t_k}) \cdot (P_{\text{rec}}^{\text{C}} \cdot t_{\text{slot}}) \\ & - \; f_{u_i}^{t_k} \cdot (P_{\text{fly}}^{\text{U}} \cdot t_{\text{slot}}) \\ & - \; \sum_{s_j \in S} \left(w_{i,j}^{t_k} \cdot P_{\text{wu}} \cdot t_{\text{slot}} \right) \\ & - \; \text{su}_{u_i}^{t_k} \cdot P_{\text{startup}}^{\text{U}} \cdot t_{\text{slot}} \\ & - \; r_{u_i}^{t_k} \cdot \left(\left(\text{com}_{\text{tx},u_i}^{t_k} \cdot P_{\text{tx}}^{\text{U}} \right) + \left(\text{com}_{\text{rx},u_i}^{t_k} \cdot P_{\text{rx}}^{\text{U}} \right) \right) \cdot t_{\text{slot}} \end{aligned}$$

Here, $P_{\text{rec}}^{\text{C}}$ is the power of recharging station $c_i \in C$ (uniform hardware is assumed in both cases), and $P_{\text{fly}}^{\text{U}}$ is the average propulsion power of UAVs where we assume comparable energy consumption for the hovering and flying phases because of the presence of very low number of UAV acceleration/deceleration actions and limited UAV speed [42]. Similarly, the energy update rule for each WGS is defined as follows:

$$\begin{aligned} E(s_j, t_k) = \; & E(s_j, t_{k-1}) & (9) \\ & - \; E_{\text{self}}^{\eta} \left(E(s_j, t_{k-1}), t_{\text{slot}} \right) \\ & - \; \text{su}_{s_j}^{t_k} \cdot P_{\text{startup}}^{\text{S}} \cdot t_{\text{slot}} \\ & - \; r_{s_j}^{t_k} \cdot \left(\left(\text{com}_{\text{tx},s_j}^{t_k} \cdot P_{\text{tx}}^{\text{S}} \right) + \left(\text{com}_{\text{rx},s_j}^{t_k} \cdot P_{\text{rx}}^{\text{S}} \right) \right) \cdot t_{\text{slot}} \end{aligned}$$

Here, E_{self}^{η} is the energy loss function during each time slot due to the self-discharge process that is battery-characteristic (monthly loss rate equal to $\eta\%$ is assumed):

$$E_{\text{self}}^{\eta}(e, t) = e \cdot \left(1 - \left(\left(\frac{100 - \eta}{100}\right)^{\frac{t}{60 \cdot 60 \cdot 24 \cdot 30}}\right)\right) \tag{10}$$

5. Optimization Problem

Based on the system model previously introduced, the goal of this study is to determine the joint WGS wake-up scheduling and the UAV path-planning (i.e. the $f_{u_i}^{t_k}$, $w_{i,j}^{t_k}$ and $r_{[u_i,s_j]}^{t_k}$ functions), so that the optimal trade-off between the WSN lifetime and the Value of Sensing (VoS) gathered by the UAVs is achieved. To this aim, we assume that the primary goal of the IoT data collection is the coverage, i.e. to produce periodic snapshots on how the sensed quantity is varying over the scenario. The WGSs can be distributed in any mode (uniform distribution is not assumed). However, we assume that: (*i*) all the WGSs are identical, i.e. they measure the same quantity with the same accuracy; (*ii*) the sensed quantity exposes local spatial correlations among different locations of the environment; (*iii*) the sensed quantity might vary over time.

More in details, we denote with $\mathcal{T} = \{\tau_{i,j}^{t_k}, \cdots\}$ the set of all the sensor readings gathered by the UAV $u_i \in U$, and with $\tau_{i,j}^{t_k}$ the sensor value sent by $s_j \in S$ to the UAV at time slot t_k where $\text{tr}_{i \leftarrow j}^{t_k} = 1$. In order to quantify the VoS of each sensor reading $\tau_{i,j}^{t_k} \in \mathcal{T}$, we introduce the cost function $\mathcal{L}_C : \mathcal{T} \to [0..1]$ defined as follows:

$$\mathcal{L}_C\left(\tau_{i,j}^{t_k}\right) = \max_{\substack{0 \leq w < k \\ u_l \in U \\ s_x \in S}} \left(\text{tr}_{l \leftarrow x}^{t_w} \cdot \mathcal{L}_S\left(s_j, s_x\right) \cdot \mathcal{L}_T\left(t_k, t_w\right)\right) \tag{11}$$

$$\mathcal{L}_S\left(s_i, s_j\right) = \frac{1}{1 + e^{(\text{d}_{2D}(s_i, s_j) - m_s) \cdot k_s}} \tag{12}$$

$$\mathcal{L}_T\left(t_i, t_j\right) = \frac{1}{1 + e^{(|t_i - t_j| - m_t) \cdot k_t}} \tag{13}$$

Here, the $\mathcal{L}_C$ function is a proxy for the data correlation, and it quantifies the relevance of each sensor reading $\tau_{i,j}^{t_k}$ executed before time slot t_k when compared with: (*i*) sensor data produced by other WGSs and already gathered by the UAVs (*spatial* correlation expressed by Equation 12) and (*ii*) earlier sensor data from any WGS (*temporal*

22

correlation expressed by Equation 13). More in details, the spatial correlation function $\mathcal{L}_S$ quantifies the relevance of the current sensor measurement $\tau_{i,j}^{t_k}$ based on the euclidean distance from the measurements already gathered by the UAVs. Vice versa, the temporal correlation function $\mathcal{L}_T$ reflects the freshness of the data, considering the time elapsed since the last sensor reading, similar to [9]. In the Equations above, m_s, k_s, m_t, and k_t are user-defined coefficients modeling the shape of the loss functions.

Based on the loss function $\mathcal{L}_C$, we introduce the VoS utility function Ψ, defined as follows:

$$\Psi = \sum_{k=1}^{T_{\text{LIMIT}}} \sum_{u_i \in U} \sum_{s_j \in S} \text{tr}_{i \leftarrow j}^{t_k} \cdot \left(1 - \mathcal{L}_C(\tau_{i,j}^{t_k})\right) \tag{14}$$

Finally, the optimization problem can be formally described as follows:

$$\text{find} \quad \text{f}_{u_i}^{t_k}, \text{w}_{i,j}^{t_k}, \text{r}_{[u_i,s_j]}^{t_k}, p(u_i, t_k), \varrho(u_i, t_k)$$

$$\text{maximize} \quad \Psi$$

subject to the energy constraints defined by Equations 8 and 9, the energy update rule of Equation 5, and to the following constraints:

$$\text{d}_{\text{3D}}(p(u_i, t_k), p(u_i, t_{k-1})) \leq v_{\max} \cdot t_{\text{slot}} \tag{15}$$

$$\text{d}_{\text{2D}}(p(u_i, t_k), p(u_i, t_{k-1})) \cdot \left(1 - (\text{f}_{u_i}^{t_k} \cdot \text{f}_{u_i}^{t_{k-1}})\right) = 0 \tag{16}$$

$$\text{d}_{\text{2D}}(p(u_i, t_k), p(c_i)) \cdot (1 - \text{f}_{u_i}^{t_k}) = 0 \tag{17}$$

$$\text{d}_{\text{2D}}(\text{hov}(u_i, s_j, t_k), p(s_j)) \cdot \text{w}_{i,j}^{t_k} \leq h_{u_i}^{t_k} \cdot \tan \frac{\min(\alpha_{\max}^U, \alpha_{\max}^S)}{2} \tag{18}$$

$$(1 - \text{f}_{u_i}^{t_k}) \cdot h_{u_i}^{t_k} = 0 \tag{19}$$

$$(1 - \text{f}_{u_i}^{t_k}) + \sum_{s_j \in S} \text{w}_{i,j}^{t_k} + \text{su}_{u_i}^{t_k} + \text{r}_{u_i}^{t_k} \leq 1 \tag{20}$$

$$\text{off}_{u_i}^{t_k} \cdot (1 - \text{su}_{s_j}^{t_k}) \cdot (1 - \text{r}_{s_j}^{t_k}) + \text{on}_{s_j}^{t_k} \cdot \left(\text{su}_{s_j}^{t_k} + \text{r}_{s_j}^{t_k}\right) = 1 \tag{21}$$

23

$$(1 - \text{su}_{u_i}^{t_k}) + (\text{su}_{u_i}^{t_k} \cdot (\text{su}_{u_i}^{t_{k-1}} + \sum_{s_j \in S} \text{w}_{i,j}^{t_{k-1}})) = 1 \tag{22}$$

$$(1 - \text{su}_{s_j}^{t_k}) + (\text{su}_{s_j}^{t_k} \cdot (\text{su}_{s_j}^{t_{k-1}} + E_{\text{check}}^{s_j}(t_{k-1}))) = 1 \tag{23}$$

$$\left(1 - \text{w}_{i,j}^{t_k}\right) \cdot E_{\text{acc}}^{s_j}(t_k) = 0 \tag{24}$$

$$\sum_{s_j \in S} \text{w}_{i,j}^{t_k} \leq 1 \quad \forall u_i \in U \tag{25}$$

$$\sum_{u_i \in U} \text{w}_{i,j}^{t_k} \leq 1 \quad \forall s_j \in S \tag{26}$$

$$(1 - \text{r}_{[u_i,s_j]}^{t_k}) + \left(\text{r}_{[u_i,s_j]}^{t_k} \cdot (\text{r}_{[u_i,s_j]}^{t_{k-1}} + \text{su}_{[u_i,s_j]}^{t_{k-1}})\right) = 1 \tag{27}$$

$$\text{r}_{[u_i,s_j]}^{t_k} \cdot \text{su}_{[u_i,s_j]}^{t_{k-1}} \cdot \left(\prod_{l=k-\text{t}_{\text{startup}}}^{k-1} \text{su}_{[u_i,s_j]}^{t_l}\right) +$$
$$+ (1 - \text{r}_{[u_i,s_j]}^{t_k}) + (1 - \text{su}_{[u_i,s_j]}^{t_{k-1}}) \geq 1 \tag{28}$$

$$\text{off}_{s_j}^{t_k} \cdot \text{on}_{s_j}^{t_{k-1}} \cdot \left(\prod_{l=k-(n_r \cdot \text{t}_{\text{timeout}})}^{k-1} \text{r}_{s_j}^{t_l}\right) + \text{on}_{s_j}^{t_k} + \text{off}_{s_j}^{t_{k-1}} \geq 1 \tag{29}$$

$$(1 - \text{r}_{u_i}^{t_k}) \cdot \text{r}_{u_i}^{t_{k-1}} \cdot \left(\left(\prod_{l=k-(n_r \cdot \text{t}_{\text{timeout}})}^{k-1} \text{r}_{s_j}^{t_l}\right) +$$
$$+ \left(\sum_{s_j \in S} \text{tr}_{i \leftarrow j}^{t_{k-1}}\right)\right) + \text{r}_{u_i}^{t_k} + (1 - \text{r}_{u_i}^{t_{k-1}}) \geq 1 \tag{30}$$

$$\text{com}_{[\text{rx,tx}],[u_i,s_j]}^{t_k} \cdot \text{r}_{[\text{rx,tx}],[u_i,s_j]}^{t_k} +$$
$$+ (1 - \text{com}_{[\text{rx,tx}],[u_i,s_j]}^{t_k}) \cdot (1 - \text{r}_{[\text{rx,tx}],[u_i,s_j]}^{t_k}) = 1 \tag{31}$$

$$\text{com}_{\text{tx},u_i}^{t_k} \cdot \left(\text{su}_{u_i}^{t_{k-1}} + \text{com}_{\text{tx},u_i}^{t_k - t_{\text{timeout}}}\right) + \left(1 - \text{com}_{\text{tx},u_i}^{t_k}\right) = 1 \tag{32}$$

$$\text{tr}_{i \to j}^{t_k} \cdot \text{com}_{\text{tx},u_i}^{t_k} \cdot \text{com}_{\text{rx},s_j}^{t_k} + \left(1 - \text{tr}_{i \to j}^{t_k}\right) = 1 \tag{33}$$

$$\text{tr}_{i \leftarrow j}^{t_k} \cdot \text{com}_{\text{rx},u_i}^{t_k} \cdot \text{com}_{\text{tx},s_j}^{t_k} + \left(1 - \text{tr}_{i \leftarrow j}^{t_k}\right) = 1 \tag{34}$$

$$\text{tr}_{i \leftarrow j}^{t_k} \cdot \left(1 - \prod_{l=k-t_{\text{timeout}}+1}^{k-1} \left(1 - \text{tr}_{i \to j}^{t_k}\right)\right) + \left(1 - \text{tr}_{i \leftarrow j}^{t_k}\right) = 1 \tag{35}$$

$$E(u_i, t_k) > 0 \tag{36}$$

$$E(s_j, t_k) > 0 \tag{37}$$

where all the previous constraints apply $\forall u_i \in U$, $\forall c_i \in C$, $\forall s_j \in S$, and $\forall t_k \leq T_{\text{LIMIT}}$. Here, constraint 15 limits the UAV speed to $v_{\max}$; constraints 16 and 17 state that the UAV cannot change its position while recharging, during the take-off and the landing; constraint 18 states that the UAV can transfer energy to a WGS only if it is hoovering in the radiating cone of the WGS's antenna; constraint 19 states that the UAV altitude while recharging is equal to zero; constraints 20 and 21 ensure that the states w, su and r are mutually disjoint; constraints 22 and 23 ensure that the UAVs and the WGSs can enter state su only after the wake-up operation (UAVs) or after being activated (WGSs); constraint 24 states that the accumulated energy of a WGS not activated by any UAV is zero; constraints 25 and 26 state that the UAV can wake-up only one WGS at each time-slot, and that a WGS can receive energy by only one UAV at each time-slot; constraints 27 and 28 ensure that the state r follows state su for t_{startup} time slots; constraint 29 ensures that the WGS remains in communication state for $n_r \cdot t_{\text{timeout}}$ time slots, and constraint 30 sets the analogous condition for the UAV; constraints 31, 32, 33 and 34 ensure that the data exchange will happen in state r and that the UAV and the WGS will use the correct mode for transmitting and receiving the data packets; constraint 35 states that any REPLY-ACK message can be sent only after

25

the REQUEST one and within t_{timeout} time slots; finally constraints 36 and 37 limit the lifetime of both WGSs and UAVs.

6. BEE-DRONES Algorithms

The optimization problem described in the previous Section requires a deterministic knowledge of how the scenario will evolve over time, since both the controller and the environmental errors (e.g. the $\varrho(u_i, t_k)$, $\vec{e}_{\text{HOVER}}(u_i, s_j, t_k)$ and $\vec{e}_{\text{LOC}}(u_i, s_j, t_k)$ variables) are defined on a per-slot basis. Since such fine-grained modeling is clearly unfeasible, we propose to decompose the research problem into three stages:

- *Stage I*. We assume that the UAV controller and the environmental conditions will not change during the mission task. Hence, we replace the per-slot variables modeling the UAV hovering process (e.g. the $\varrho(u_i, t_k)$, $\vec{e}_{\text{HOVER}}(u_i, s_j, t_k)$, $\vec{e}_{\text{LOC}}(u_i, s_j, t_k)$ and $\vec{e}_{\text{POS}}(u_i, s_j, t_k)$ variables) with probability distributions. In this work we assume these latter as zero mean normal distributions with variance equal to σ_R^2, σ_{HOVER}^2, σ_{LOC}^2 and $\sigma_{\text{POS}}^2 = \sigma_{\text{HOVER}}^2 + \sigma_{\text{LOC}}^2$, respectively. In addition, we introduce two thresholds, i.e.: (*i*) ξ, defined as the minimal requested probability that the data-transfer between the WGS and the UAV will occur successfully and (*ii*) ζ, defined as the requested probability that the wake-up procedure will end successfully. Both the thresholds above are user-defined, and provided as input to the optimization problem. Based on them, we compute t_{opt} and h_{opt}, i.e. respectively the minimal hovering time and maximal height of the UAVs guaranteeing that the: (*i*) the UAV will activate the WGS within t_{opt} time-slots with probability at least equal to ξ; (*ii*) the UAV will successfully receive the REPLY-ACK message with probability greater or equal than ζ. For readability reasons, we moved the details on how t_{opt} and h_{opt} can be computed on the Appendix Appendix A.

- *Stage II*. We transform the joint scheduling and planning problem of Section 5 into a multi-commodity flow problem on a multi-graph (Section 6.1). Here, vertexes of the graph correspond to the stop positions of the UAVs (i.e. on a

26

charging station or hovering over a WGS), while arcs correspond to the actions that can be performed by the UAVs (i.e. flying, recharging, transferring energy or communicating with the WGSs).

- *Stage III*. We introduce a centralized, iterative heuristic that computes the itinerary of each UAV on the multi-graph data structure (Section 6.2). The proposed solution assumes global scenario knowledge but de-synchronized operations of the UAVs; i.e., each time a UAV reaches a charging station, its charging duration and the next flight itinerary are computed by taking into account the WGSs already visited by the other UAVs and their current itineraries. Then, we further refine such heuristic with a distributed solution that removes the assumption of global knowledge and relies on local communication among the UAVs (Section 6.3).

6.1. Multi-graph formulation

We model the UAVs and WGSs operations by using a multiperiod directed multi-graph $G(V, A)$. Here, the set of nodes V is composed by pairs (q_i, t_k), where and $q_i \in S \cup C$ is a stop position of the UAV (i.e. charging or hovering) and $t_k \in T$. The set A denotes the arcs of the multi-graph; here, each element $a_j \in A$ is defined as a pair $[(q_i, t_k), (q'_i, t'_k)]_l$, where (q_i, t_k) is the tail of the arc and (q'_i, t'_k) its head. Moreover, each arc is characterized by an energy cost denoted as $W(a_i)$. We distinguish among seven different arc types (denoted by the subscript l):

- *charge arc*: $[(c_i, t_k), (c_i, t_{k+1})]_{\mathrm{rec}} \in A_{\mathrm{rec}} \subset A$, with $c_i \in C$, this arc type models the charging operations at station c_i during time slot t_k; in this case $W(a_i) = P^U_{\mathrm{rec}} \cdot t_{\mathrm{slot}}$.

- *fly arc*: $[(q_i, t_k), (q'_i, t'_k)]_{\mathrm{fly}} \in A_{\mathrm{fly}} \subset A$, with $q_i \neq q'_i$, this arc type models the action of flying from node q_i at time slot t_k to another q'_i, with time of arrival equal to t'_k. In this case $W(a_i) = -P^U_{\mathrm{fly}} \cdot t_{\mathrm{slot}} \cdot (t'_k - t_k)$.

- *irradiation arc*: $[(s_j, t_k), (s_j, t'_k)]_{\mathrm{irr}} \in A_{\mathrm{irr}} \subset A$, with $s_j \in S$, where $(t'_k - t_k) \cdot t_{\mathrm{slot}} = t_{\mathrm{irr}}$; this arc type models the action of energy transfer towards WGS s_j; in this case $W(a_i) = -(P^U_{\mathrm{fly}} + P^U_{\mathrm{wu}}) \cdot t_{\mathrm{irr}}$.

- *communication arc*: $[(s_j, t_k), (s_j, t'_k)]_{\text{com}} \in A_{\text{com}} \subset A$, with $s_j \in S$, where $(t'_k - t_k) \cdot t_{\text{slot}} = t_{\text{startup}} + n_r \cdot t_{\text{timeout}}$. This arc type models the sensor data gathering from WGS s_j. To this purpose, we force a UAV to wait for the full request/reply procedure before moving towards the next WGS of its itinerary; moreover, without loss of generality, we assume that the reading $\tau_{s_j}^{t'_k}$ occurs at time slot t'_k:

$$W(a_i) = - P_{\text{fly}}^U \cdot t_{\text{slot}} \cdot (t'_k - t_k) \tag{38}$$
$$- \text{wu}_{h_{\text{opt}}, t_{\text{opt}}} \cdot \big(P_{\text{startup}}^U \cdot t_{\text{startup}}$$
$$+ \left(P_{\text{rx}}^U + \frac{P_{\text{tx}}^U - P_{\text{rx}}^U}{t_{\text{timeout}}} \right) \cdot n_r \cdot t_{\text{timeout}} \big)$$

where $\text{wu}_{h_{\text{opt}}, t_{\text{opt}}}$ is the wake-up probability, defined in Appendix Appendix A.

- *off arc*: $[(s_j, t_k), (s_j, t_{k+1})]_{\text{off}} \in A_{\text{off}} \subset A$, with $s_j \in S$, this arc type indicates that WGS s_j is in *off* state; in this case $W(a_i) = -P^\eta(E_{\max}^S, t_{k+1}) \cdot t_{\text{slot}}$, where P^η denotes the power loss due to the battery self-discharge process, and it can be derived from Equation 10.

- *on arc*: $[(s_j, t_k), (s_j, t'_k)]_{\text{on}} \in A_{\text{on}} \subset A$, with $s_j \in S$, this arc type indicates that WGS s_j is in *on* state, where $(t'_k - t_k) \cdot t_{\text{slot}} = t_{\text{startup}} + n_r \cdot t_{\text{timeout}}$; in this case:

$$W(a_i) = - P^\eta(E_{\max}^S, t'_k) \cdot t_{\text{slot}} \cdot (t'_k - t_k) \tag{39}$$
$$- \text{wu}_{h_{\text{opt}}, t_{\text{opt}}} \cdot \big(P_{\text{startup}}^S \cdot t_{\text{startup}}$$
$$+ \left(P_{\text{rx}}^S + \frac{P_{\text{tx}}^S - P_{\text{rx}}^S}{t_{\text{timeout}}} \right) \cdot n_r \cdot t_{\text{timeout}} \big)$$

In the *communication* and *on* arcs, $\text{wu}_{h_{\text{opt}}, t_{\text{opt}}}$ denotes the probability that a UAV hovering for t_{opt} time-slots is activating a WGS from a ground height of h_{opt} meters; details on how the $\text{wu}_{h_{\text{opt}}, t_{\text{opt}}}$ function is derived are provided in the Appendix A. For modeling purpose, we added the following elements to the graph: (*i*) a sink node s, representing the destination of all the flows, and (*ii*) a set of terminal arcs $[(q_i, T_{\text{LIMIT}}), s]_{\text{ter}} \in A_{\text{ter}} \subset A, \forall q_i \in S \cup C$ connecting all the terminal nodes to the sink with zero energy cost, i.e. $W([(q_i, T_{\text{LIMIT}}), s]_{\text{ter}}) = 0, \forall q_i \in S \cup C$. We modeled

28

the action selection process of each UAV u_i through the following *non-splittable flow variables* set:

$$\varphi^{u_i}_{[(q_j,t_k),(q'_j,t'_k)]_l} \in \Phi = \begin{cases} 1 & \text{if } u_i \text{ uses } [(q_j,t_k),(q'_j,t'_k)]_l \\ & \text{and } l \in \{\text{rec, fly, irr, com, ter}\} \\ 0 & \text{otherwise} \end{cases} \qquad (40)$$

and for each WGS s_j:

$$\varphi^{s_j}_{[(q_i,t_k),(q'_i,t'_k)]_l} \in \Phi = \begin{cases} 1 & \text{if } s_j \text{ uses } [(q_i,t_k),(q'_i,t'_k)]_l \\ & \text{and } q_i = q'_i = s_j \text{ and } l \in \{\text{on, off, ter}\} \\ 0 & \text{otherwise} \end{cases} \qquad (41)$$

Finally, we rewrite the goal function of Equation 14 and the overall optimization problem as follows:

$$\Psi_{\text{MF}} = \sum_{u_i \in U} \sum_{a=[(s_j,t_k),(s_j,t'_k)]_{\text{com}} \in A_{\text{com}}} \varphi^{u_i}_a \cdot \left(1 - \mathcal{L}_{\mathcal{C}}(\tau^{t'_k}_{i,j})\right) \qquad (42)$$

$$\text{find} \qquad \varphi^a_{[(q_j,t_k),(q'_j,t'_k)]_l} \qquad \text{with } a \in U \cup S$$

$$\text{maximize} \qquad \Psi_{\text{MF}}$$

subject to the following constraints:

$$\sum_{[(\phi,\tau),(q_j,t_k)]_l \in A} \varphi^a_{[(\phi,\tau),(q_j,t_k)]_l} - \sum_{[(q_j,t_k),(\phi,\tau)]_l \in A} \varphi^a_{[(q_j,t_k),(\phi,\tau)]_l}$$

$$= \text{BAL}_{(q_j,t_k),a}, \quad \forall(q_j,t_k) \in V, a \in U \cup S \qquad (43)$$

$$E(a,t_k) = E(a,t_{k-1}) + \sum_{[(\phi,\tau),(q_j,t_k)]_l \in A} W([(\phi,\tau),(q_j,t_k)]_l) \cdot \varphi^a_{[(\phi,\tau),(q_j,t_k)]_l})$$

$$\forall a \in U \cup S, t_k \in T \qquad (44)$$

$$\sum_{u_i \in U} \sum_{[(s_j,t_k),(s_j,t'_k)]_{\text{com}} \in A_{\text{com}}} \varphi^{u_i}_{[(s_j,t_k),(s_j,t'_k)]_{\text{com}}} = \qquad (45)$$

$$= \sum_{[(s_j,t_k),(s_j,t'_k)]_{\text{on}} \in A_{\text{on}}} \varphi^{s_j}_{[(s_j,t_k),(s_j,t'_k)]_{\text{on}}} \qquad \forall s_j \in S, t_k \in T$$

29

$$\sum_{c_j \in C, i \neq j} \varphi^{u_i}_{[(c_j,t_k),(c_j,t_{k+1})]_{\mathrm{rec}}} = 0 \qquad \forall u_i \in U, t_k \in T \tag{46}$$

$$\mathrm{zl}_a^{t_k} \leq \mathrm{zl}_a^{t_{k+1}} \qquad \forall a \in U \cup S, t_k \in T \tag{47}$$

$$\mathrm{zg}^{t_k} \leq \mathrm{zg}^{t_{k+1}} \qquad \forall t_k \in T \tag{48}$$

$$\mathrm{zl}_a^{t_k} \leq \mathrm{zg}^{t_k} \qquad \forall a \in U \cup S, t_k \in T \tag{49}$$

$$E(a, t_k) + M \cdot \mathrm{zl}_a^{t_k} \geq 0 \qquad \forall a \in U \cup S, t_k \in T \tag{50}$$

$$\varphi^{u_i}_{[(s_j,t_k),(s_j,t_k')]_{\mathrm{com}}} \leq 1 - \mathrm{zg}^{t_k} \quad \forall u_i \in U, s_j \in S, t_k \in T \tag{51}$$

$$\varphi^{u_i}_{[(c_i,t_0),(c_i,t_1)]_{\mathrm{rec}}} = 1 \quad \forall u_i \in U \tag{52}$$

$$\varphi^{s_j}_{[(s_j,t_0),(s_j,t_1)]_{\mathrm{off}}} = 1 \quad \forall s_j \in S \tag{53}$$

Constraint (43) is the (fundamental) flow conservation constraint. Here, the value of $\mathrm{BAL}_{(q_j,t_k),a}$ depends on the considered node, i.e.:

1. for nodes $(q_j, t_0) \in V$, $\mathrm{BAL}_{(q_j,t_0),a}$ is equal to -1 if the UAV/WGS is in q_j at time t_0 (flow sources);

2. for all nodes $(q_j, t_k) \in V$ such that $k > 0$, $\mathrm{BAL}_{(q_j,t_k),a}$ is equal to 0, since they are crossed by the UAVs/WGSs and hence they have a null balance;

3. for the sink node s, $\mathrm{BAL}_{s,a} = 1$, $\forall a \in U \cup S$, since it represents the destination of all the flows.

Constraint (44) is the energy update function, that slightly differs from Equations 8 and 9 since we consider the worst case where the UAV receives the REP-ACK message after n_r attempts. Constraint (45) ensures that maximum one UAV is communicating

with WGS s_j at each time slot. Constraint (46) states that each UAV u_i can recharge only at its charging station c_i. Constraints (47, 48, 49, 50) model the event of system failure (i.e. when at least one UAV or WGS runs out of energy) through the *local status-off variables* (zl) and the *global status-off variable* (zg):

$$zl_a^{t_k} = \begin{cases} 1 & \text{if } a \in U \cup S \text{ is off in } t_k, \text{ i.e. } E(a, t_k) \le 0 \\ 0 & \text{otherwise} \end{cases} \tag{54}$$

$$zg^{t_k} = \begin{cases} 1 & \text{if any } a \in U \cup S \text{ is off in } t_k \\ 0 & \text{otherwise} \end{cases} \tag{55}$$

The conditions above also ensure that the residual energy of each UAV/WGS is always greater then zero at each t_k, until the global status-off variable is activated (here M is an arbitrary integer coefficient, much greater then $E_{\max}^U$ and $E_{\max}^S$). Constraint (51) ensures that no sensor reading occurs when at least one UAV or WGS has run out of energy. Finally, constraints (52, 53) initialize the flows at time slot t_0, i.e. the UAV u_i is starting from its charging station (c_i, t_0) and the WGS s_j from node (s_j, t_0).

6.2. *Centralized Heuristic*

In the optimization problem defined so far, there is an implicit trade-off between the the correlation of the sensor readings and the amount of data gathered by the UAVs over time, i.e. the WSN lifetime. We make such trade-off explicit, by slightly modifying the VoS function for each UAV sensor reading $\tau_{i,j}^{t_k} \in \mathcal{T}$ in this way:

$$\mathcal{L}_{\text{BEE}}\left(\tau_{i,j}^{t_k}\right) = \mathcal{L}_C\left(\tau_{i,j}^{t_k}\right) \dot{+} \mathcal{L}_E\left(\tau_{i,j}^{t_k}\right) \tag{56}$$

Where $\dot{+}$ symbol indicates the algebraic sum defined as $a \dot{+} b = a + b - ab$. Here, the first addendum $\mathcal{L}_C$ is the spatial correlation function defined in Equation 11, and the second addendum, i.e. $\mathcal{L}_E$ is a proxy for the WSN lifetime, ensuring that all the WSGs are discharged at the same rate, i.e.:

$$\mathcal{L}_E\left(\tau_{i,j}^{t_k}\right) = 1 - \left(\frac{E(s_j, t_k) - \min_{s_l \in S}(E(s_l, t_k))}{\max_{s_l \in S}(E(s_l, t_k)) - \min_{s_l \in S}(E(s_l, t_k))}\right) \tag{57}$$

31

Algorithm 1: The BEE-DRONES centralized algorithm

Input: U, S, C, G, Φ

1   $\varphi^{u_i}_{[(c_i,t_0),(c_i,t_1)]_{\text{rec}}} \in \Phi \leftarrow 1; \quad \forall c_i \in C, \forall u_i \in U$

2   $\varphi^{s_j}_{[(s_j,t_k),(s_j,t_{k+1})]_{\text{off}}} \in \Phi \leftarrow 1; \quad \forall s_j \in S, \forall t_k \in T$

3   **while** *true* **do**

4    $[u_i, t_k] \leftarrow \texttt{LeftmostIdleUAV}(G, \Phi)$

5   **if** $t_k \geq T_{\text{LIMIT}}$ *or* *CheckWGSsEnergy(*G, Φ, t_k*)* **then**

6   **break**

7   **end**

8   path $\leftarrow \texttt{MultiflowPath}(G, \Phi, u_i, t_k)$

9    $\texttt{UpdateUAVFlowVariables}(G, \Phi, \text{path}, u_i)$

10   $\varphi^{s_j}_{[(s_j,t_{k''}),(s_j,t_{k''+1})]_{\text{on}}} \leftarrow 1; \forall (q_{i'}, t_{k'}) \rightarrow (s_j, t_{k''}) \in \text{path}$

11   **end**

12   **return** Φ

Algorithm 2: The $\texttt{LeftmostIdleUAV}$ function

Input: G, Φ

1   $A_{\max} \leftarrow \emptyset$

2   **forall** $u_i \in U$ **do**

3    $\varphi^{u_i}_{[(c_i,t_k),(c_i,t_{k+1})]_{\text{rec}}} \leftarrow \text{argmax}_{a \in A_{\text{rec}}} (\varphi^{u_i}_a \cdot t_k))$

4    $A_{\max} \leftarrow A_{\max} \cup \varphi^{u_i}_{[(c_i,t_k),(c_i,t_{k+1})]_{\text{rec}}}$

5   **end**

6   $\varphi^{u_i}_{[(c_i,t_k),(c_i,t_{k+1})]_{\text{rec}}} \leftarrow \text{argmin}_{a \in A_{\max}} (\varphi^{u_i}_a \cdot t_k))$

7   **return** $[u_i, t_{k+1}]$

Algorithm 3: The `MultiflowPath` function

Input: G, Φ, u_i, t_k

1   $k' \leftarrow k$; $e \leftarrow E(u_i, t_k)$;

2   **while** $(t_{k'} < T_{\mathrm{LIMIT}})$ **and** $(e \leq E^U_{\max})$ **do**

3      $[\mathrm{path}_{k'}, g_{k'}] \leftarrow$ `BSFMultiFlow`$(G, \Phi, u_i, t_{k'}, e)$

4      $e \leftarrow e + W([(c_i, t_{k'}), (c_i, t_{k'+1})]_{\mathrm{rec}})$

5      $k' \leftarrow k' + 1$

6   **end**

7   $k^* \leftarrow \mathrm{argmax}_{k \leq k^* < k'}(g_{k^*})$

8   $\varphi^{u_i}_{[(c_i, t_{k'}), (c_i, t_{k'+1})]_{\mathrm{rec}}} \leftarrow 1; \forall k \leq k' < k^*$

9   **return** path_{k^*}

The centralized heuristic is based on the multi-graph data structure described in the previous Section; it determines the path of each UAV until any WGS runs out of battery or the requested WSN lifetime T_{LIMIT} is achieved. The optimal path of the UAV fleet can be computed through a complete exploration of the multi-graph, hence considering all possible combinations of the actions of the UAVs over time; however, this approach is clearly unfeasible due to the high computational cost. For this reason, we propose an iterative heuristic which computes the path of each UAV, by splitting it into *episodes*; each episode is composed of an initial recharging phase (i.e. a sequence of time-slots during which UAV u_i recharges its battery at c_i) and a *feasible* path, defined as a list of WGSs to wake-up. Each feasible path for UAV u_i starts and ends necessarily at c_i, i.e. the charging station. For each possible duration of the charging phase, we explore the multi-graph via a revised Breadth-First Search (BFS) technique with pruning rules, in order to keep the complexity always polynomial in N_S, i.e. the number of WGSs. The feasible path minimizing the cost $\mathcal{L}_{\mathrm{BEE}}$ is selected for the current episode of the target UAV. The heuristic proceeds by determining the episode of the next UAV, while keeping track of the set of WGSs visited so far, so that the $\mathcal{L}_C$ and $\mathcal{L}_E$ correlation factors are properly updated. The technical details of the proposed centralized heuristic are provided below.

Algorithm 4: The `BSFMultiFlow` function

Input: G, Φ, u_i, t_k, e

1 $\mathrm{path}(u_i, t_k) \leftarrow \emptyset; \Phi(u_i, t_k) \leftarrow \Phi$

2 $R((u_i, t_k)) \leftarrow e; L \leftarrow \{(u_i, t_k)\}; g((u_i, t_k)) \leftarrow 0$

3 $Q.enqueue((u_i, t_k))$

4 **while** *(not Q.empty)* **do**

5 $\quad (q_{i'}, t_{k'}) \leftarrow Q.dequeue$

6 $\quad$ **forall** $s_j \neq q_{i'}$ *ascending ordered by* $\mathcal{L}_{\mathrm{BEE}}^{\Phi(q_{i'}, t_{k'})}(\tau_{s_j}^{t_m})$ *with* $m \leftarrow k' + F[q_{i'}, s_j]$ **do**

7 $\quad\quad$ **if** $R((q_{i'}, t_{k'})) - D[q_{i'}, s_j] - D[s_j, c_i] > 0$ **and** $\mathrm{path}((s_j, t_m)) = \emptyset$ **then**

8 $\quad\quad\quad Q.enqueue((s_j, t_m))$

9 $\quad\quad\quad \mathrm{path}(s_j, t_m) \leftarrow \mathrm{path}(q_{i'}, t_{k'}) + (s_j, t_m)$

10 $\quad\quad\quad R((s_j, t_m)) \leftarrow R((q_{i'}, t_{k'})) - D[q_{i'}, s_j]$

11 $\quad\quad\quad g((s_j, t_m)) \leftarrow g((q_{i'}, t_{k'})) + \left(1 - \mathcal{L}_{\mathrm{BEE}}^{\Phi(q_{i'}, t_{k'})}(\tau_{s_j}^{t_m})\right)$

12 $\quad\quad\quad \Phi(s_j, t_m) \leftarrow \Phi(q_{i'}, t_{k'})$

13 $\quad\quad\quad \varphi_{[(q_{i'}, t_{k'}), (s_j, t_m)]_{\mathrm{fly}}}^{u_i} \in \Phi(s_j, t_m) \leftarrow 1$

14 $\quad\quad\quad L \leftarrow L \setminus \{(q_{i'}, t_{k'})\}; L \leftarrow L \cup \{(s_j, t_m)\}$

15 $\quad\quad\quad$ **if** $L.size > N_S$ **then**

16 $\quad\quad\quad\quad (s, t) \leftarrow \underset{(s,t) \in L}{\mathrm{argmin}} \left(g((s,t))\right)$

17 $\quad\quad\quad\quad L \leftarrow L \setminus \{(s, t)\}$

18 $\quad\quad\quad\quad Q.remove((s, t))$

19 $\quad\quad\quad$ **end**

20 $\quad\quad$ **end**

21 $\quad$ **end**

22 **end**

23 $(s, t) \leftarrow \underset{(s,t) \in L}{\mathrm{argmax}} \left(g((s,t))\right)$

24 **return** $[\mathrm{path}(s, t), g((s, t))]$

The pseudo-code of the heuristic is described by Algorithm 1. First, the φ set is initialized (lines 1, 2), by assuming that all the UAVs are in charging state and the WGSs are switched off. The iterative procedure works by computing the episode of each UAV in isolation; to this aim, the leftmost UAV u_i in the multi-graph G is selected (function LeftmostIdleUAV in Algorithm 2), till any WGS runs out of energy (checked by the function CheckWGSsEnergy) or the time limit is reached (line 5 of Algorithm 1). The function MultiflowPath (defined by Algorithm 3) returns the path for UAV u_i, starting from time slot t_k: for each possible duration of the charging time and before reaching the time limit (line 2 of Algorithm 3) the minimum-cost feasible path is computed. The best calculated path is returned as result of the procedure (lines 7 and 9 of Algorithm 3) and the multiflow variables are updated accordingly (line 8 of Algorithm 3). As previously stated, a path is said feasible whether it originates from the node $(c_i, t_k) \in V$ (i.e. from the charging station), includes only WGS nodes $(s_j, t_{k*}) \in V$ and terminates on a charging node $(c_i, t_{k**}) \in V$, with the UAV residual energy always positive at each intermediate node. The feasible paths from each starting node $(c_i, t_k) \in V$ are computed by the function BSFMultiFlow (Algorithm 4), which properly explores the multi-graph data structure, through a variation of the Breadth-First Search (BFS) algorithm. Like in legacy BSF, a queue (Q) is used to keep the list of nodes that need to be explored at the current layer; however pruning mechanisms are used in order to limit the number of active exploration paths to the number of WGSs (N_S). In the BSFMultiFlow procedure, the variable $\text{path}(q,t)$ stores the calculated path toward the initial node (c_i, t_k); $R((q,t))$ is the residual UAV energy at node (q,t); L is the set of active paths; $\Phi(q,t)$ is a temporary copy of the original flow variables Φ used to keep track of the visited WGSs; $g((q,t))$ is the total gain of path $\text{path}(q,t)$. At each level, the BSF visits the WGSs in an ascending order based on the total gain (line 6 of Algorithm 4); here $\mathcal{L}_{\text{BEE}}^{\Phi(q,t)}$ defines the reading loss based on the temporary flow variables set $\Phi(q,t)$. At each exploration of node $(s_j, t_{k*}) \in V$, we check the feasibility of the path by ensuring that the residual energy of the UAV is enough to reach the WGS s_j and then the charging station c_i; in case, the WGS s_j is added to the path (lines 8-14 of Algorithm 4). In line 15-19 of Algorithm 4 we implement the pruning mechanism: if the number of active paths is grater then the threshold N_S, the path with

35

the lowest gain value (line 16 of Algorithm 4) is removed from the queue. Then, the path with maximum gain among the available N_S is selected (line 23 of Algorithm 4). Finally, in lines 9 and 10 of Algorithm 1 the flow variables are updated according to the calculated path. Here, the UpdateUAVFlowVariables procedure updates the flow variables φ^{u_i} belonging to the fly, irr and com classes.

Computational complexity

The computational complexity of Algorithm 1, CC($Algorithm$ 1), is determined by the main loop (line 3 of Algorithm 1) where, at each round, the method MultiflowPath is invoked in the worst case, n_{path} times, i.e. until T_{LIMIT}. It is easy to notice that: $n_{\text{path}} = \frac{t_{\text{LIMIT}}}{E_{\max}^U/P_{\text{rec}}^C + E_{\max}^U/P_{\text{fly}}^U}$. The total computational cost is then CC($Algorithm$ 1) $= \mathcal{O}(N_U \cdot n_{\text{path}} \cdot$ CC(MultiflowPath)). The CC(MultiflowPath) executes the BSFMultiFlow function while recharging and then it chooses the minimum cost path. The loop at line 2 of Algorithm 3 is executed at maximum $n_{\text{rec}} = \frac{E_{\max}^U}{P_{\text{rec}}^C \cdot t_{\text{slot}}}$ times, hence: CC(MultiflowPath) $=$ $\mathcal{O}(n_{\text{rec}} \cdot$ CC(BSFMultiFlow)). The CC(BSFMultiFlow) is dominated by the *while* loop (line 4 of Algorithm 4) that is used to traverse the multi-graph. Let us define Lev $= \frac{E_{\text{MAX}}^U}{P_{\text{fly}}^U \cdot (d_{\text{avg}}/v_{\max})}$ as the average number of WGSs that an UAV can visit in a single path, where d_{avg} is the average distance between two WGSs. In the legacy BSF algorithm, the number of visited arcs grows exponentially over the number of levels Lev, i.e. $\mathcal{O}(N_S^{\text{Lev}})$. However, through the pruning mechanism, only N_S paths are active (line 15 of Algorithm 4) and hence the number of arcs visited is $\mathcal{O}(N_S \cdot \text{Lev})$. While visiting the arcs, the algorithm computes the reading losses and then orders the WGSs list based on the loss values (line 6 of Algorithm 4). The $\mathcal{L}_{\text{BEE}}$ function can be executed in $\mathcal{O}(N_S)$[6], while the ordering procedure has a cost of $\mathcal{O}(N_S \cdot$ $\log_2(N_S))$. Hence, the total cost of the command at line 6 of Algorithm 4 is $\mathcal{O}(N_S \cdot$ $\log_2(N_S) + N_S^2) = \mathcal{O}(N_S^2)$. Hence, the total cost of the BSFMultiFlow procedure is CC(BSFMultiFlow) $= \mathcal{O}(N_S^3 \cdot \text{Lev})$, and the overall computational cost

---

[6]We assume that the most affecting reading in the loss calculation (i.e. the last one) is stored for each WGS.

of *Algorithm 1* is $\mathrm{CC}(Algorithm\,1) = \mathcal{O}(N_U \cdot n_{\mathrm{path}} \cdot n_{\mathrm{rec}} \cdot N_S^3 \cdot \mathrm{Lev})$. Hence, the computational cost is polynomial over the number of WGSs and of UAVs.

6.3. Distributed heuristic

The centralized algorithm described in the previous Section assumes global scenario knowledge and coordination among the UAVs, and the presence of a static number of UAVs in the field; however, this assumption might not hold due to UAV failures and/or to UAV additions. To this purpose, we propose here a distributed method that works similarly to the centralized one, except that it is executed locally on each UAV. At the system startup, the UAVs are not aware of the presence of other peers. Hence, each UAV computes its path on the multi-graph data structure, that is populated with local information only. In order to avoid uncoordinated actions with multiple UAVs activating the same sequence of WGSs, the following enhancement is introduced: the UAVs periodically broadcast their current path on the wireless channel. When receiving a message from another peer, a priority rule is used to merge the information on the multi-graph of the UAV with the lowest priority; the path with the list of the next WGSs to visit is re-calculated accordingly.

The technical details of the proposed heuristic are shown in Algorithm 5. Each UAV calculates a feasible path through the `MultiflowPath` function (line 9). If no feasible path is found, then the UAV u_i keeps recharging at c_i (lines 10-12). Otherwise, the UAV u_i follows the path by visiting the WGSs (lines 14-21) and moving at its charging station at the end of the episode (lines 22-23). We assume that the information exchange happens when two UAVs u_i and u_q are at a distance lower than d_{com}, which models the radio propagation range of the UAVs. When meeting UAV u_q, the UAV u_i broadcasts at time t_k a beacon message with the following information: $\mathrm{BEACON}_i = \langle \Phi_i, U_i \rangle$, where $U_i = \{\langle u_i, c_i, E(u_i, t_k) \rangle, \dots\}$ is the set of known UAVs, their charging station positions and their actual residual energy. When receiving the BEACON_q message from the UAV u_q, the UAV u_i invokes the `MeetWhileFlying` function (line 1): a priority check is performed by considering the residual energy of both devices. If $E(u_q, t_k) < E(u_i, t_k)$, i.e. UAV u_q has the highest priority (line 18), then UAV u_i adds the received data to its local multi-graph

37

Algorithm 5: The BEE-DRONES Distributed heuristic

Input: u_i, S, c_i, G, Φ_i

1 Function MeetWhileFlying(Φ_q, U_q)**:**

2 $U_i \leftarrow U_i \cup U_q$

3 $\Phi_i \leftarrow \Phi_i \cup \Phi_q$

4 return

5 $k \leftarrow 0$

6 $l_i \leftarrow c_i$

7 $U_i \leftarrow \{\langle u_i, c_i \rangle\}$

8 while *true* **do**

9   path $\leftarrow$ MultiflowPath(G, Φ_i, u_i, t_k)

10   **if** path $= \emptyset$ **then**

11 $\varphi^{u_i}_{[(c_i,t_k),(c_i,t_{k+1})]_{\mathrm{rec}}} \leftarrow 1$

12 $k \leftarrow k + 1$

13   **else**

14   **while** $(s_j, t_m) \leftarrow getNext(\text{path})$ **do**

15 $\varphi^{u_i}_{[(l_i,t_k),(s_j,t_m)]_{\mathrm{fly}}} \leftarrow 1$

16 $k \leftarrow m$

17 $l_i \leftarrow s_j$

18   **if** *CheckChanged(Φ_i)* **then**

19   path $\leftarrow$ MultiflowPath(G, Φ_i, s_j, t_k)

20   **end**

21   **end**

22 $\varphi^{u_i}_{[(l_i,t_k),(c_i,t_{k+F[l_i,c_i]})]_{\mathrm{fly}}} \leftarrow 1$

23 $k \leftarrow k + F[l_i, c_i]$
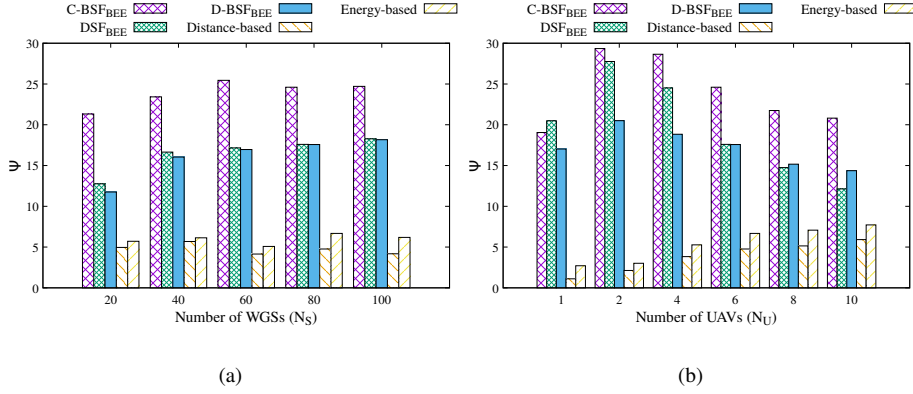
24   **end**

25 end

Figure 6: The utility function Ψ for T_{LIMIT}=1 day and varying numbers of WGSs and UAVs is shown in Figure 6(a) and 6(b), respectively.

data structure, and recomputes its current path accordingly.

Computational complexity

The computational complexity is determined by the $\mathrm{CC}(\texttt{MultiflowPath})$ method: $\mathrm{CC}(Algorithm\ 5) = \mathcal{O}(n_{\mathrm{rec}} \cdot N_S^3 \cdot \mathrm{Lev})$, where n_{rec} is the number of executed loops in $\texttt{MultiflowPath}$ and Lev is the average number of WGSs that an UAV can visit in a single path. We can see that Algorithm 5 is polynomial over the number of WGSs.

7. Experimental results

In this Section, we evaluate the system performance of the BEE-DRONES framework by simulating the scenario presented in Section 4 and the WGS/UAV operations via the OMNeT++ tool. Unless stated otherwise, we used the following parameters: $M = 10\ Km$ is to simulate a large-scale scenario; $P_{\mathrm{wu}} = 27\ dBm$, $f = 868 MHz$, $E^{\mathrm{WU}} = 633.6\ nJ$, $G_{\max}^U = 7.3\ dBi$, $G_{\max}^S = 1\ dBi$, $\alpha_{\max}^U = \pi/4$, and $\alpha_{\max}^S = \pi/2$ are the parameters used and measured during the experiments presented in Section 3; $P_{\mathrm{rec}}^C = 20\ W$, $P_{\mathrm{fly}}^U = 4 \cdot 21.7\ W$, $E_{\max}^S = 4\ kJ$ (300 mAh at 3.7 V battery), $E_{\max}^U = 120\ kJ$ (3000 mAh at 11.1 V battery), $\eta = 8\%$, $v_{\max} = 12\ m/s$, and $d_{\mathrm{com}} = 100\ m$ describe a generic quadcopter having 4 brushless motors equipped with a 3000 mAh battery with $\sim$23 min flight time, on the average; we used an
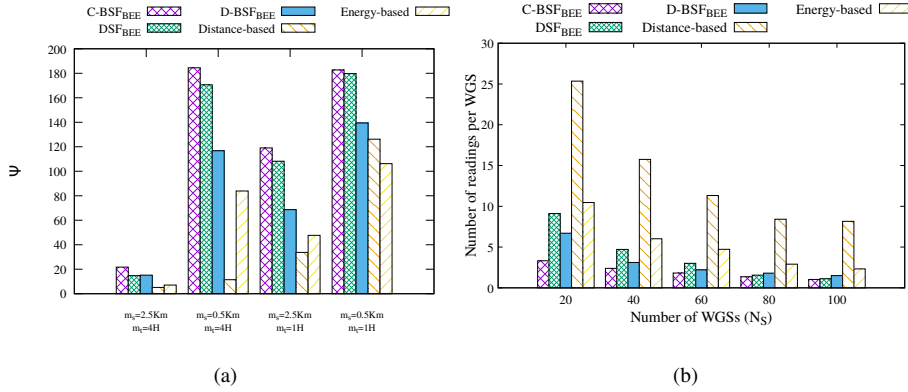
39

Figure 7: In Figure 7(a) we show the impact of different correlation parameters (m_s and m_t). The average number of readings for T_{LIMIT}=1 day and varying numbers of WGSs is shown in Figure 7(b).

high value $\eta = 8\%$ as self-discharge parameter (actual Li-Po batteries have 2-3% self-discharge value) in order to speed-up the simulations, without invalidating them. $P_{\text{startup}}^S = P_{\text{startup}}^U = 5\ mW$, $P_{\text{tx}}^S = P_{\text{tx}}^U = 100\ mW$, $P_{\text{rx}}^S = P_{\text{rx}}^U = 10\ mW$, $t_{\text{slot}} = 0.2\ s$, $t_{\text{startup}} = 1\ s$, $t_{\text{timeout}} = 1\ s$, and $n_r = 3$ are used to simulate the communication model described in Section 4.4. $m_s = 2.5\ km$, $k_s = 0.004$, $m_t = 4\ h$, $k_t = 0.0006$, $\xi = \zeta = 0.9$ describe the correlation model for the sensor's readings. Here, we described sensors, like air temperature/humidity sensors, that have low spatial correlation (below 0.1) at distance over $3\ km$ and low temporal correlation after $5\ h$. Finally, $T_{\text{LIMIT}} = 1$ day, $N_S = 80$, $N_U = 6$, $\sigma_{\text{POS}}^2 = 1$, $\sigma_R^2 = \pi/128$. Based on the parameters ξ and ζ, and by using Equations A.10 and A.11, we derived $h_{\text{opt}} = 6.6\ m$ and $t_{\text{opt}} = 5$. We set consequently $t_{\text{irr}} = t_{\text{opt}} \cdot t_{\text{slot}}$.

We compare the performance of centralized BEE-DRONES (C–BSF_{BEE}) of Section 6.2, and distributed BEE-DRONES (D–BSF_{BEE}) of Section 6.3, against the following algorithms: (*i*) DSF_{BEE}, i.e. a centralized version of Algorithm 1 that is using the *depth-first* search on a single path, rather than the *breadth-first* search on N_S paths; (*ii*) *Distance-based* heuristic, which builds the path of each UAV in a greedy way by selecting the closest WGS at each step; (*iii*) *Energy-based* heuristic, which -similar to the previous case- builds the path of each UAV by selecting the WGS with the lowest residual energy at each step. Similarly to C–BSF_{BEE}, both the *Distance-based* and the
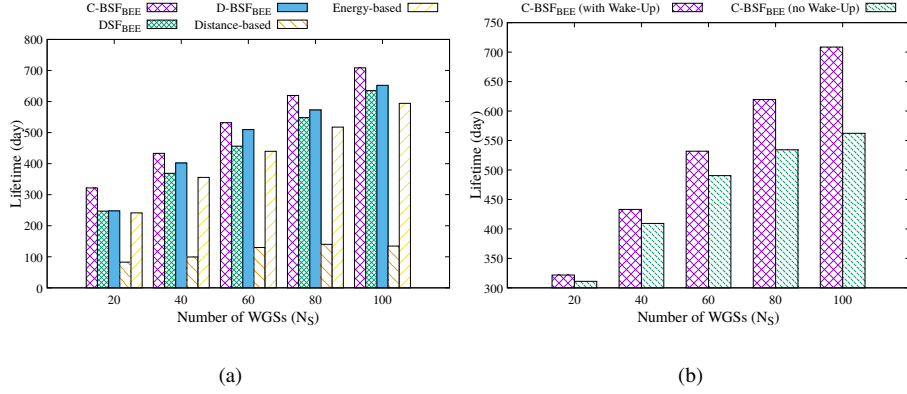
40

Figure 8: The system lifetime for varying numbers of WGSs and $T_{\mathrm{LIMIT}} = \infty$ is depicted in Figure 8(a). The system lifetime when comparing the Wake-up Radio (WR) and the Duty-Cycle (DC) technologies is depicted in Figure 8(b).

Energy-based algorithms explore the multi-flow graph using the BSF algorithm; however, the distance metric and the residual energy metric are used in the exploring step (line 6) of Algorithm 1, respectively. It is easy to notice that the *Distance-based* solution aims to maximize the number of sensor readings performed by the UAVs, while the *Energy-based* solution aims to maximize the WSN lifetime.

In Figure 6(a), we show the utility function Ψ when varying the number N_S of WGSs for a fixed number of UAVs $N_U = 6$. Generally speaking, the Ψ values slightly increase for the C–BSF$_{\mathrm{BEE}}$ schemes when increasing N_S, since higher numbers of WGSs translate into lower temporal correlation values of the sensor readings. In addition, we can notice that: (*i*) the proposed centralized C–BSF$_{\mathrm{BEE}}$ overcome all the other path-planning strategies; (*ii*) the distributed version D–BSF$_{\mathrm{BEE}}$ behaves similarly to the DSF$_{\mathrm{BEE}}$, and in any case it greatly overcomes both the *Distance-based* and the *Energy-based* for all values of N_S.

The results shown in Figure 6(a) can be compared with those in Figure 7(b), where the average number of per-WGS sensor readings is shown. The *Distance-based* and *Energy-based* schemes produce the highest values of sensor readings; however, they do not maximize the VoS, since several readings are correlated in both time and space, and hence they could be considered unnecessary. Vice versa, the C–BSF$_{\mathrm{BEE}}$ schemes
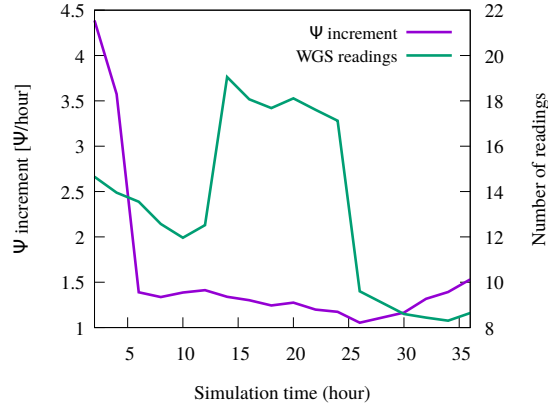
41

Figure 9: The Ψ/time values and the number of WGS readings in a dynamic scenario where the number of available UAVs varies during the simulation (D–BSF$_{\mathrm{BEE}}$ algorithm is used).
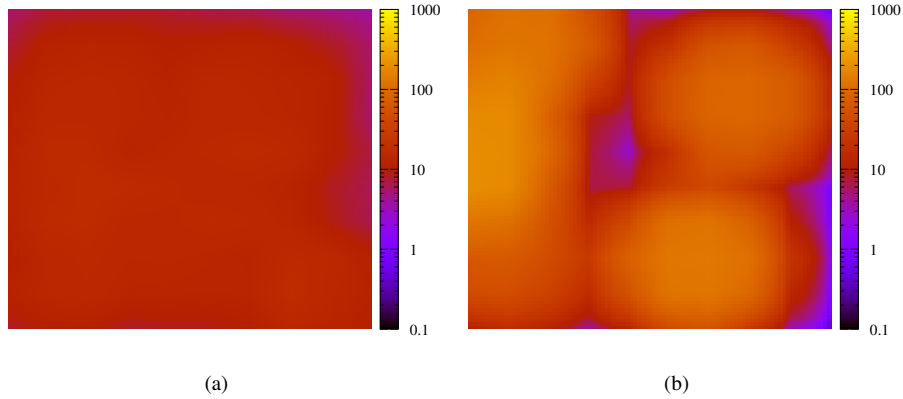

(a)　　　　　　　　　　　　　　　(b)

Figure 10: The heatmaps showing the scenario coverage for the BSF$_{\mathrm{BEE}}$ centralized algorithm and the *Distance-based* algorithm are showed in Figure 10(a) and Figure 10(b), respectively.

performs a careful WGS selection by balancing the requirements of the sensing application (e.g. area coverage) with the system lifetime. This is also made evident in Figure 6(b) that shows the utility function Ψ when varying the number N_U of UAVs, for a fixed number of $N_S = 80$ WGSs. Also in this case, the C–BSF$_{\mathrm{BEE}}$ algorithms maximize the VoS compared to the *Distance-based* and *Energy-based* schemes, while the DSF$_{\mathrm{BEE}}$ algorithm does not scale with a large number of UAVs. Furthermore, we can notice an interesting saturation effect for the utility function Ψ, i.e. given N_S and

42

the specific correlation parameters in use ($w_s = 2.5km$ and $w_t = 4H$), there exists an optimal number of UAVs ($N_U = 2$ in this case) maximizing the Ψ function. The utility function decreases when adding more UAVs (in our case $N_U > 2$). The motivation is that -regardless of the path-planning scheme- too many UAVs in the scenarios will reduce the quality of the data gathered by increasing the average correlation of the sensor readings. To this purpose, Figure 7(a) shows the value of the utility faction Ψ for different correlation parameters w_s and w_t (on the $x-$axis). Lowering these parameters translates into an increase of the Φ metric for all the schemes. However, even under different correlation parameters, the C–BSF$_{\mathrm{BEE}}$ algorithm is able to maximize the VoS against the competitors. In Figure 8(a) we show the the system lifetime, i.e. the time-slot in which the first WGS runs out of energy. In this case we set $T_{\mathrm{LIMIT}} = \infty$. We can notice that - when increasing the number of WGSs in the scenario- the C–BSF$_{\mathrm{BEE}}$ algorithms produce significant improvements also compared to the *Energy-based* solution; indeed, this latter involves more sensor readings with respect to BEE-DRONES (see Figure 7(b)) and hence it drains the battery of the WGSs faster. In Figure 8(b), we provide further insights on the energy efficiency of our proposal, by comparing the usage of the wake-up radio (WR) technology against classical duty-cycle (DC) mechanism that sets the WGS in sleep mode during idle phases. For the DC consumption in sleep mode, we used the experimental values reported in Table 1 (i.e. $10\mu W$). Since the focus of the analysis is on the WGS technology, and not on the path-planning strategy, we used C–BSF$_{\mathrm{BEE}}$ in both cases. The lifetime increment produced by the WR technology is remarkable, and it achieves the 30% for N_S=100. Also, we assume in this analysis that the WGSs using the DC mode are able to perfectly synchronize their duty cycles with the UAVs hovering over them, which is unfeasible in real-world scenarios; vice-versa, no synchronization issues occur in case the WR technology is used. Figure 9 shows the adaptiveness of the distributed algorithm D–BSF$_{\mathrm{BEE}}$ in a scenario characterized by a time-varying number of UAVs; on the y axis we depict the Ψ gain over time, while on the $y2$ axis there is the average number of per-WGS sensor readings. At the system startup, we set $N_U = 6$; at time $t = 12H$ we added two more UAVs ($N_U = 8$) and finally at time $24H$ we simulate the failure of 4 UAVs ($N_U = 4$). As expected, the number of readings follows the number of available UAVs. However,

43

we can see the effectiveness of the UAV coordination in the WGS selection, which translates into a fast adaptation of the Ψ gain. Also, how previously depicted in Figure 6(b), there is a saturation issue when $N_U > 6$, while for $N_U = 4$ the Ψ gain increases. Finally, Figures 10(a) and 10(b) demonstrates the ability of BEE-DRONES algorithms to provide adequate scenario coverage. More specifically, the heatmaps show the areas of the scenario where the sensor data are acquired by the UAVs; the color of each location is related to the number of sensor readings performed by the UAVs. We compared C–BSF$_{BEE}$ (Figure 10(a)) with *Distance-based* (Figure 10(b)). In this experiment $N_S = 80$ and $N_U = 6$. As expected the *Distance-based* method is able to gather more sensor data, however it concentrates its operations on few areas (i.e. those closer to the charging stations). On the other side, the C–BSF$_{BEE}$ algorithm provides a more uniform coverage of the target area, by balancing the readings over the WGSs.

8. Conclusions

In this paper, we proposed BEE-DRONES, a novel framework for the deployment of ultra low-power UAV-aided Wireless Sensor Networks (WSNs) on large-scale IoT scenarios. The utilization of Wake-up Radio (WR) technology has been proposed in order to address the synchronization problem between the UAVs and the Wireless Ground Sensors (WGSs); to this purpose, the effectiveness of WR technology has been tested via measurements under different power and antenna configurations. Then, we moved from the UAV-WGS link to the UAV-WSN scenario, and we formulated the research problem of the optimal path-planning strategies for the UAVs which must gather sensing data from WR-based WGSs: differently from other studies, the optimization framework takes into account the lifetime of the WGSs, the energy constraints of the UAVs, and the Value of Sensing (VoS) data gathered by the application. Both centralized and distributed heuristics have been proposed and evaluated through OMNeT++ simulations. The experimental results demonstrate that both centralized and distributed BEE-DRONES solutions are able to maximize the VoS when compared with greedy path-planning strategies. Also, they are able to greatly increase the system lifetime with respect to Duty-Cycle (DC) technology. Future works include: the realization
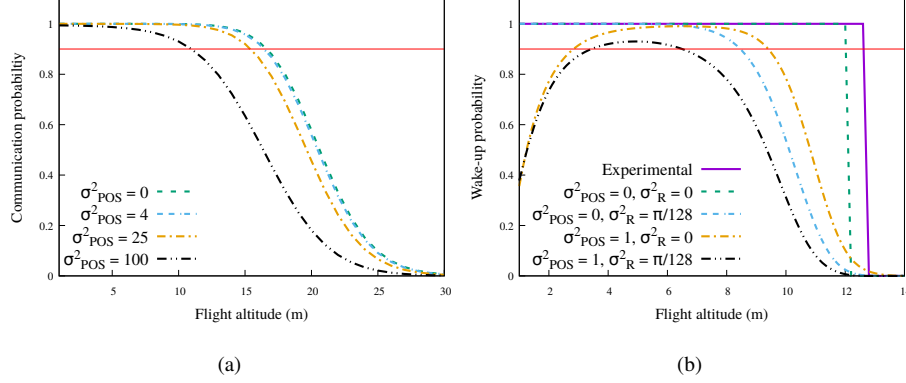
44

(a)   (b)

Figure .11: The successful data communication probability with probability of packet loss $\mathbb{P}_{\text{pl}}(d_{3\text{D}}) = 1 - \frac{1}{1 + e^{(d_{3\text{D}} - 20) \cdot 0.3}}$ is shown in Figure 11(a). The wake-up probability with $G^U_{MAX} = 7.3dBi$, $\alpha^U_{MAX} = \pi/4$, $G^S_{MAX} = 1dBi$, $\alpha^S_{MAX} = \pi/2$, $P_{\text{wu}} = 27dBm$, $t_{\text{slot}} = 0.2s$ and $T^{\text{WU}} = 5$ is shown in Figure 11(b).

of a small-case testbed of a WR-based UAV-aided WSN, the extension to a scenario
where the number of charging stations is lower than the available UAVs, the modeling
of interference on the aerial communications.

Appendix A. Derivation of the optimal flight altitude and of the optimal hovering interval for the UAVs

Let $\vec{\mathcal{E}}_{\text{LOC}} = \langle \mathcal{E}^x_{\text{LOC}}, \mathcal{E}^y_{\text{LOC}} \rangle$ be the random variable defining the localization esti-
mation error of the UAV, and $\mathcal{F}_{\vec{\mathcal{E}}_{\text{LOC}}}$ be its probability distribution function with zero
mean and variance σ^2_{LOC}. Similarly, let $\vec{\mathcal{E}}_{\text{HOVER}} = \langle \mathcal{E}^x_{\text{HOVER}}, \mathcal{E}^y_{\text{HOVER}} \rangle$ be the ran-
dom variable defining the UAV controller error and $\mathcal{F}_{\vec{\mathcal{E}}_{\text{HOVER}}}$ its probability distribu-
tion function with zero mean and variance σ^2_{HOVER}. The UAV position error is defined
as follows: $\vec{\mathcal{E}}_{\text{POS}} = \vec{\mathcal{E}}_{\text{LOC}} + \vec{\mathcal{E}}_{\text{HOVER}}$ with $\mathcal{F}_{\vec{\mathcal{E}}_{\text{POS}}}(\vec{e}) = \int_{\vec{e}' \in \mathbb{R}^2}(\mathcal{F}_{\vec{\mathcal{E}}_{\text{LOC}}}(\vec{e}') \cdot \mathcal{F}_{\vec{\mathcal{E}}_{\text{LOC}}}(\vec{e} - \vec{e}'))$ having variance $\sigma^2_{\text{POS}} = \sigma^2_{\text{LOC}} + \sigma^2_{\text{HOVER}}$. Moreover, let $\mathcal{R} = \langle \mathcal{R}_x, \mathcal{R}_y \rangle$ be the random variable defining the rotation of a UAV and $\mathcal{F}_{\mathcal{R}}$ its probabil-
ity distribution function with zero mean and variance σ^2_{R}.

Now, we determine the probability of successful data transmission between the UAV
and the WGS by using the communication protocol defined in Section 4. Let $\mathcal{D}_{3\text{D}}(h)$
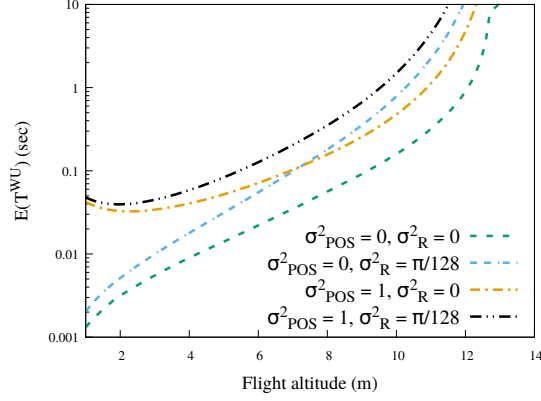
45

Figure .12: The expected time to wake-up at different flight altitude.

be the random variable that defines the 3D distance between a UAV and the actual WGS while hovering at an altitude of h:

$$\mathcal{D}_{3\mathrm{D}}(h) = \sqrt{(h)^2 + \left|\left|\vec{\mathcal{E}}_{\mathrm{POS}}\right|\right|^2} \tag{A.1}$$

The expected value of the 3D distance is:

$$\mathbb{E}(\mathcal{D}_{3\mathrm{D}}(h)) = \sqrt{(h)^2 + \int_{\vec{e} \in \mathbb{R}^2} \left(\|\vec{e}\|^2 \cdot \mathcal{F}_{\vec{\mathcal{E}}_{\mathrm{POS}}}(\vec{e})\right)} \tag{A.2}$$

We define $\mathbb{P}_{\mathrm{nodata}}(h)$ as the probability of data failure for a request/reply procedure between the WGS and the UAV flying at an altitude of h meters:

$$\mathbb{P}_{\mathrm{nodata}}(h) = 2 \cdot \mathbb{P}_{\mathrm{pl}}(\mathbb{E}(\mathcal{D}_{3\mathrm{D}}(h))) - \mathbb{P}_{\mathrm{pl}}(\mathbb{E}(\mathcal{D}_{3\mathrm{D}}(h)))^2 \tag{A.3}$$

Here, the term $\mathbb{P}_{\mathrm{pl}}(d_{3\mathrm{D}})$ indicates the data loss probability at a specific distance, and it depends from the path-loss model in use [44]. Vice versa, the probability $\mathbb{P}_{\mathrm{data}}(h)$ of successful data transmission between the UAV and the WGS can be derived as follows:

$$\mathbb{P}_{\mathrm{data}}(h) = 1 - (\mathbb{P}_{\mathrm{nodata}}(h))^{n_r} \tag{A.4}$$

where n_r is the maximum number of communication attempts. Let $h_{\max}(\xi)$ be the maximum altitude of the UAV so that the probability of successful data transmission is

46

equal or higher than the threshold ξ:

$$h_{\max}(\xi) = \underset{a \in \mathbb{R}^+}{\operatorname{argmax}} \left(\mathbb{P}_{\mathrm{data}}(a) \geq \xi \right) \tag{A.5}$$

For the energy transfer model, we introduce the conditional random variable $\mathrm{ON}^h | T^{\mathrm{wu}} = t$ that defines the event of waking up a WGS powered for t time slots by a UAV flying at an altitude h: $\mathrm{ON}^h = 1$ indicates that the WGS is activated by the UAV, $\mathrm{ON}^h = 0$ otherwise. We define the conditional wake-up probability $\mathrm{wu}_{h,t} = \mathbb{P}(\mathrm{ON}^h = 1 | T^{\mathrm{wu}} = t)$:

$$\mathrm{wu}_{h,t} = 1 - \int_0^{E^{\mathrm{WU}}} \mathbb{P}\left(E_h^{\mathrm{rx}} = e | T^{\mathrm{wu}} = t \right) de \tag{A.6}$$

The conditional variable $E_{h,t}^{\mathrm{rx}} = (E_h^{\mathrm{rx}} | T^{\mathrm{wu}} = t)$ models the total energy received by a WGS when powered by the UAV for t time slots, and its probability can be derived as follows:

$$\mathbb{P}(E_h^{\mathrm{rx}} = e | T^{\mathrm{wu}} = t) = \int \cdots \int_0^{E^{WU}} c_e(e_1, \ldots, e_t) \cdot \prod_{j=1}^t \mathbb{P}(E_{h,1} = e_j) \, de_1 \ldots de_t \tag{A.7}$$

where c_e is a check function that is equal to 1 if $e_1 + \cdots + e_t = e$, and 0 otherwise. We introduce the probability distribution function of $E_{h,1}$, which depends on the random variables $\vec{\mathcal{E}}_{\mathrm{POS}}$ and $\mathcal{R}$:

$$\mathbb{P}(E_{h,1} = e) = \iint_{-d_{2\mathrm{D}}^{\max}(e,h)}^{+d_{2\mathrm{D}}^{\max}(e,h)} \iint_{-\varrho_{\max}}^{+\varrho_{\max}} c_{\Gamma,e}(x, y, \varrho_x, \varrho_y) \cdot \tag{A.8}$$

$$\cdot \mathcal{F}_{\vec{\mathcal{E}}_{\mathrm{POS}}}(\langle x, y \rangle) \cdot \mathcal{F}_{\mathcal{R}}(\langle \varrho_x, \varrho_y \rangle) \, d\varrho_x \, d\varrho_y \, dx \, dy$$

where $c_{\Gamma,e}$ is the check function that is equal to 1 if $\Gamma(\langle x, y \rangle, \langle \varrho_x, \varrho_y \rangle, h) = e$, and 0 otherwise; $d_{2\mathrm{D}}^{\max}(e, h)$ defines the maximum 2D distance so that the UAV is able to transfer an amount of e energy from an altitude of h meters; $\varrho_{\max}$ is the maximum UAV rotation error. Based on $\mathrm{wu}_{h,t}$, we derive the duration of the energy transfer phase (i.e. the minimum number of time slots), so that the wake-up probability is higher than a threshold ζ:

$$t_{\min}^{\mathrm{wu}}(h, \zeta) = \underset{t \in \mathbb{Z}^+}{\operatorname{argmin}} \left(\mathrm{wu}_{h,t} \geq \zeta \right) \tag{A.9}$$

Finally, h_{opt} and t_{opt} can be derived as follows:

$$h_{\text{opt}} = \underset{h \leq h_{\max}(\xi)}{\operatorname{argmax}} \ (c_\zeta(h) \cdot h) \qquad (\text{A.10})$$

where $c_\zeta(h)$ is the function that is equal to 1 if exists t such that $\text{wu}_{h,t} \geq \zeta$, and 0 otherwise.

$$t_{\text{opt}} = t_{\min}^{\text{wu}}(h_{\text{opt}}, \zeta) \qquad (\text{A.11})$$

The Equations above can be solved numerically; in Figures 11(a), 11(b) and .12 we reported the impact of the flight altitude on the WGS-UAV communication and on the WGS wake-up process. More specifically, Figure 11(a) shows the probability of successful communication between the UAV and the WGS when varying the flight altitude, for different environmental conditions (σ_{POS}^2). In this case, the UAV rotation $\varrho(u_i, t_k)$ is not relevant because we assume omni-directional antenna for the data communication. As expected, the higher is the error, the lower is the maximum altitude for a successful data transmission. In Figure 11(a), the red line indicates the minimum requested probability $\xi = 0.9$. Additionally, in Figure 11(b) we show the wake-up probability for different values of σ_{POS}^2 and σ_{R}^2, when varying the flight altitude. The red reference line of $\zeta = 0.9$ denotes the altitude at which the wake-up procedure meets the user requests, i.e. $\text{wu}_{h,5} > 0.9$. In Figure 11(b) we also reported the experimental results for the static case, i.e. $\sigma_{\text{POS}}^2 = 0$ and $\sigma_{\text{R}}^2 = 0$ (see Section 3); it is easy to notice that the analytical results are very close to the experimental one. At low altitudes, the position error σ_{POS}^2 has a negative impact on the wake-up procedure due to the antenna directionality and the zenith offset between the UAV and the WGS; however, the probability increases with the altitude once the WGS enters inside the antenna irradiation cone. Finally, Figure .12 depicts the time to wake-up ($\mathbb{E}(T^{\text{WU}})$) with different rotation and position errors; as expected, the time to wake-up increases with the amount of errors.

References

[1] E. Sisinni, A. Saifullah, et al. Industrial Internet of Things: Challenges, Opportunities, and Directions. *IEEE Transactions on Industrial Informatics*, 2018.

[2] R. Piyare, A. L. Murphy, C. Kiraly, P. Tosato and D. Brunelli. Ultra low power wake-up radios: a hardware and networking survey. *IEEE Communication Surveys and Tutorials*, 19(4), pp. 2117-2157, 2017.

[3] L. Bedogni, L. Bononi, R. Canegallo, F. Carbone, M. Di Felice, E. Franchi, F. Montori, L. Perilli, T. Salmon Cinotti and A. Trotta. Dual-Mode Wake-Up Nodes for IoT Monitoring Applications: Measurements and Algorithms. *Proc. of IEEE ICC, Kansas City, USA, 2018.*

[4] S. Hayat, E. Yanmaz and R. Muzaffar. Survey on unmanned aerial vehicle networks for civil applications: a communications viewpoint. *IEEE Communications Surveys and Tutorials, 18(4), pp. 2624-2661, 2016.*

[5] M. Di Francesco, S. K. Das and G. Anastasi. Data collection in wireless sensor networks with mobile elements: a survey. *ACM Transactions on Sensor Networks, 8(1), pp. 1-31, 2011.*

[6] C. Zhan, Y. Zeng and R. Zhang. Trajectory design for distributed estimation in UAV enabled wireless sensor network. *IEEE Transactions on Vehicular Technology*. 67(10), pp. 10155 - 10159, 2018.

[7] J. Yang, X. Wang, Z. Li, P. Yang, X. Luo, K. Zhang, S. Zhang and L. Chen. Path planning of unmanned aerial vehicles for farmland information monitoring based on WSN. *Proc. of IEEE WCICA*, Guilin, China, 2016.

[8] E. Tuyishimire, A. Bagula, S. Rekhis and N. Boudriga. Cooperative data muling from ground sensors to base stations using UAVs. *Proc. of IEEE ISUT*, Heraklion, Greece, 2017.

[9] J. Liu, X. Wang, B. Bai and H. Dai. Age-optimal trajectory planning for UAV-assisted data collection. *Proc. of IEEE INFOCOM WKSHPS*, Honolulu, USA, 2018.

49

[10] J. Xu, G. Solmaz, R. Rahmatizadeh, D. Turgut and L. Boloni. Animal monitoring with unmanned aerial vehicle-aided wireless sensor networks. *Proc. of IEEE LCN*, Clearwater Beach, USA, 2015.

[11] B. Olivieri and M. Endler. An algorithm for aerial data collection from wireless sensor networks by groups of UAVs. *Proc. of IEEE IROS*, Vancouver, Canada, 2017.

[12] T. D. Ho, J. Park and S. Shimamoto. QoS contraint with prioritized frame selection CDMA MAC Protocol for WSN employing UAV. *Proc. of IEEE GLOBE-COM*, Miami, USA, 2010.

[13] S. Say, H. Inata, J. Liu and S. Shimamoto. Priority-based data gathering framework in UAV-assisted wireless sensor networks. *IEEE Sensors*, 16(4), pp. 5785-5794, 2016.

[14] A. Trotta, M. Di Felice, L. Bononi, E. Natalizio, L. Perilli, E. Franchi, T. Salmon Cinotti and R. Canegallo. BEE-DRONES: Energy-efficient Data Collection on Wake-Up Radio-based Wireless Sensor Network. *Proc. of IEEE HotSalsa, Paris, France, 2019.*

[15] H. Khodr, N. Kouzayham, M. Abdallah, J. Costantine and Z. Dawy. Energy efficient IoT sensor with RF wake-up and addressing capability. *IEEE Sensors Letters*, 1(6), pp. 1-4, 2017.

[16] R. La Rosa. RF remotely-powered integrated system to nullify standby power consumption in electrical appliances. *Proc. of IEEE IECON*, Florence, Italy, 2016.

[17] Y. Shu, H. Yousefi, P. Cheng, J. Chen, Y. Gu, T. He and K. Shin. Near-optimal velocity control for mobile charging in wireless rechargeable sensor networks. *IEEE Transactions on Mobile Computing*, 15(7), pp. 1699-1713, 2016.

[18] J. Xu, Y. Zeng and R. Zhang. UAV-enabled wireless power transfer: trajectory design and energy region characterization. *IEEE Transactions on Wireless Communications*, 2017.

50

[19]   S. Saab, A. Eid, N. Kouzayha, J. Constantine, Z. Dawy, G. Virone and F. Paonessa. UAV-enabled RF sensor wake-up. *Proc. of IEEE CAMA*, Vasteras, Sweden, 2018.

[20]   M. Bacco, E. Ferro and A. Gotta. UAVs in WSNs for agricultural applications; an analysis of the two-ray radio propagation model. *Proc. of IEEE SENSORS*, Valencia, Spain, 2014.

[21]   X. Ma, R. Kacimi and R. Dhaou. Adaptive hybrid MAC protocols for UAV-assisted mobile sensor networks. *Proc. of IEEE CCNC*, Las Vegas, USA, 2018.

[22]   S. Mori. Cooperative sensing data collecting framework by using unmanned aircraft vehicle in wireless sensor network. *Proc. of IEEE ICC*, Kuala Lumpur, Malaysia, 2016.

[23]   A. Giorgetti, M. Lucchi, M. Chiani and M. Z. Win. Throughput per pass for data aggregation from a wireless sensor network via a UAV. *IEEE Transactions on Aerospace and Electronic Systems*, 47(4), pp. 2610-2627, 2011.

[24]   R. Sugihara and R. K. Gupta. Optimizing energy-latency trade-off in sensor networks with controlled mobility. *Proc. of IEEE INFOCOM*, Rio De Janeiro, Brazil, 2009.

[25]   Y. Qin, D. Boyle and E. Yeatman. A novel protocol for data links between wirless sensors and UAV based sink nodes. *Proc. of IEEE WF-IoT*, Singapore, 2018.

[26]   J. Gong, T.-H. Chang, C. Shen and X. Chen. Aviation time minimization of UAV for data collection from energy constrained sensor networks. *Proc. of IEEE WCNC*, Barcelona, Spain, 2018.

[27]   S. Liu, Z. Wei, Z. Guo, X. Yuan and Z. Feng. Performance analysis of UAVs assisted data collection in wireless sensor network. *Proc. of IEEE VTC Spring*, Porto, Portugal, 2018.

[28]   A. Wichmann, J. Chester and T. Korkmaz. Smooth path construction for data mule tours in wireless sensor networks. *Proc. of IEEE Globecom*, Anaheim, USA, 2012.

51

[29] C. Y. Tazibt, M. Bekhti, T. Djamah, N. Achir and K. Boussetta. Wireless sensor network clustering for UAV-based data gathering. *Proc. of IEEE Wireless Days*, Porto, Portugal, 2017.

[30] D.-T. Ho, E. I. Grotli, P. B. Sujit, T. A. Johansen and J. B. De Sousa. Performance evaluation of cooperative relay and particle swarm optimization path planning for UAV and wireless sensor network. *Proc. of IEEE GLOBECOM*, Atlanta, USA, 2013.

[31] S. Rashed and M. Soyturk. Effects of UAV mobility patterns on data collection in wireless sensor networks. *Proc. of IEEE COMNETSAT*, Bandung, Indonesia, 2015.

[32] G. Murtaza, S. Kanhere and S. Jha. Priority-based coverage path planning for aerial wireless sensor networks. *Proc. of IEEE ISSNIP*, Melbourne, Australia, 2013.

[33] C. Zhan, Y. Zeng and R. Zhang. Energy-efficient data collection in UAV enabled wireless sensor network. *IEEE Wireless Communications Letters*, 7(3), pp. 328-331, 2017.

[34] Q. Yang and S.-J. Yoo. Optimal UAV path planning: sensing data acquisition over IoT sensor networks using multi-objective bio-inspired algorithms. *IEEE Access*, 6(1), pp. 13671-13684, 2018.

[35] X. Liu, T. Xi, E. Ngai and W. Wang. Path planning for aerial sensor networks with connectivity constrains. *IEEE ICC*, Paris, France, 2017.

[36] O. S. Oubbati, A. Lakas, F. Z., M. Gne and M. B. Yagoubi. A survey on position-based routing protocols for Flying Ad hoc Networks (FANETs). *Vehicular Communications*, 10, pp. 29-56, 2017.

[37] A. Bujari, C.E. Palazzi and D Ronzani. A comparison of stateless position-based packet routing algorithms for FANETs. *IEEE Transactions on Mobile Computing*, 17(11), pp. 2468-2482, 2018.

[38] A. Bujari, C. Calafate, J. C. Cano, P. Manzoni, C.E. Palazzi and D Ronzani. A location-aware waypoint-based routing protocol for airborne DTNs in search and rescue scenarios. *Sensors*, 18 (11), 2018.

[39] R. L. Rosa, G. Zoppi, L. Di Donato, G. Sorbello, C. A. Di Carlo and P. Livreri. A Battery-Free Smart Sensor Powered with RF Energy. *Proc. of IEEE RTSI*, Palermo, Italy, 2018.

[40] A. Trotta, M. Di Felice, F. Montori, K. R. Chowdhury and L. Bononi. Joint Coverage, Connectivity, and Charging Strategies for Distributed UAV Networks. *IEEE Transactions on Robotics*, 34(4): 883-900, 2018.

[41] G. Calcev, M. Dillon. Antenna Tilt Control in CDMA Networks. *Proc. of 2nd annual international workshop on Wireless internet (WICON '06)*, ACM, New York, NY, USA, 2006.

[42] Y. Zeng, J. Xu and R. Zhang. Energy Minimization for Wireless Communication With Rotary-Wing UAV. *IEEE Transactions on Wireless Communications*, 18(4): 2329-2345, 2019.

[43] Rappaport, Theodore S. Wireless communications: Principles and Practice. Vol. 2. New Jersey: prentice hall PTR, 1996.

[44] A. A. Khuwaja, Y. Chen, N. Zhao, M.-S. Alouini, Paul Dobbins A Survey of Channel Modeling for UAV Communications. *IEEE Communications Survey & Tutorials*, 20(4): 2804-2821, 2018.